Experimental study of composite cold-formed steel and timber flooring systems with innovative shear connectors

Nathan Vella [a], Pinelopi Kyvelou [b], Spiridione Buhagiar [c], Leroy Gardner [d]

[a] Department of Civil and Structural Engineering, University of Malta, MSD 2080
Email: *nathan.vella@um.edu.mt* (Corresponding author)

[b] Department of Civil and Environmental Engineering, Imperial College London, SW7 2AZ
Email: *pinelopi.kyvelou11@imperial.ac.uk*

[c] Department of Civil and Structural Engineering, University of Malta, MSD 2080
Email: *spiridione.buhagiar@um.edu.mt*

[d] Department of Civil and Environmental Engineering, Imperial College London, SW7 2AZ
Email: *leroy.gardner@imperial.ac.uk*

Abstract

An experimental investigation into the structural response of cold-formed steel-timber composite flooring systems with innovative and irregularly spaced shear connectors is presented in this paper. Five composite beam tests and a series of supporting material and push-out tests were carried out. The obtained results showed that the innovative shear connectors enabled the generation of considerable composite action, resulting in up to about 45% increases in load-carrying capacity and 15% and 20% increases in the initial and mid-range stiffnesses respectively over the non-composite system. Methods for predicting the effective flexural stiffness and moment capacity of the examined cold-formed steel-timber composite beams are presented and validated against the derived physical test data. It is shown that accurate predictions for both the flexural stiffness and moment capacity can be obtained, with mean prediction-to-test ratios of 0.93 and 0.91 respectively.

Keywords: Composite beam tests, cold-formed steel, effective flexural stiffness, innovative shear connectors, testing, timber particle board.

1. Introduction

Flooring systems composed of cold-formed steel (CFS) beams supporting timber boards are widely used in construction, particularly in industrial and commercial applications. Retrofitting of mezzanine floor plates and the replacement of damaged slabs are examples of typical situations where use of these flooring systems is preferred, due to their dry construction method, ease of installation facilitated by the lightweight, easily transportable and manoeuvrable nature of the components, high strength-to-weight ratio and the possibility for demountability and reuse [1-7]. Lightweight floor plates can, however, be prone to excessive deflections and vibrations due to their low flexural stiffness, while CFS beams are susceptible to local and distortional instabilities due to the slender nature of the cross-sections, limiting their ultimate load-carrying capacity [5, 6, 8]. Recent studies [8-12] have shown that these drawbacks can be mitigated by harnessing the composite action that can potentially develop between the timber boards and the CFS beams. Composite action shifts the position of the neutral axis such that a smaller proportion of the CFS section is in compression [10, 12], while the connectors linking the two components provide partial restraint to the CFS compression flange, thus delaying the development of local and distortional instabilities [13]. Composite action also enhances the flexural stiffness of the system, hence reducing vibrations and deflections. The shift of the neutral axis and the increase in flexural stiffness are dependent on the degree of composite action, which is in turn dependent on the strength and slip modulus of the interface connection [9, 14].

Current practice is for timber boards to be connected to the underlying CFS beams via self-drilling screws, inserted at regular intervals, typically with one screw per board. The advantage of using such screws is mainly the fast installation process, with the screws being drilled from the top of the floorboard into the steel, eliminating the need for access from the underside while

ensuring an intrinsically safe working environment. Initial studies on CFS-timber flooring systems have therefore mainly focussed on self-drilling screws used as connectors [8-10, 14], examining how their spacing influences the structural behaviour of the system.

Seeking to enhance the shear connection and, hence, the composite action in CFS-timber flooring systems, the authors, motivated by previous studies on timber-to-timber [15-22] and timber-to-concrete connections [23-29], carried out research to investigate the impact of adopting inclined screws [30]. The study showed that, although there are significant benefits derived from the inclined screw configuration, these can be offset by the level of difficulty encountered when installing the screws on-site. This led the authors to develop innovative shear connectors that can be easily installed on-site and can enhance the strength and slip modulus of the connection [31, 32].

The aim of the present study is to investigate the behaviour of the best performing innovative shear connectors developed in [32] when installed on a CFS-timber flooring system subjected to bending. The study also assesses analytical solutions which may be used to predict the ultimate strength and effective flexural stiffness of the composite system. It should be noted that this study focuses on the performance of the connectors and, therefore, the proportions of the CFS beams [33] and of the wood-based particle boards were kept constant throughout the investigation. In practice, variations in the timber or CFS components may affect the behaviour, performance and ultimately the failure mode of the shear connectors.

2. Material and shear connector tests

The shear connection is key to the efficiency of a composite system; therefore, previous research carried out by the authors [30, 32, 34] was aimed at investigating and developing an understanding of the complex interactions at the shear interface. An overview of the conducted tests is given in Sections 2.1 and 2.2, and the key results are presented in Tables 1, 2 and 3. The innovative connectors that have been employed in the composite beam tests presented herein are described in Section 2.3.

2.1. Material and interaction tests

The first category of tests carried out in [30] was aimed at determining the material properties of the constituent components of the CFS-timber flooring system, namely the CFS beams, the boards, and the connectors.

The compressive properties of the wood-based particle boards were determined in accordance with BS EN 789:2004 [35]. Compression tests were carried out on 380 mm long, 100 mm wide and 76 mm deep particle board specimens and the results, presented in Table 1, were in close agreement with those of previous testing [9] carried out on the same timber product.

Tensile tests, according to BS EN ISO 6892-1:2016 [36], were carried out on the second component of the flooring system being investigated, the CFS beams. Tensile coupons were extracted from the webs, flanges, and corners of the CFS beams, as shown in Fig. 1. The tensile test results presented in Table 1 are the weighted average results for the flat and corner regions.

The third component of the composite flooring system, the connectors, were ordinary self-drilling screws of 5.5 mm diameter. Tensile tests according to BS EN ISO 898-1 [37] and BS EN ISO 6892-1:2016 [36], and bending tests according to ASTM F1575-17 [38] were carried

out and the average results are summarised in Table 1. Note that no additional material tests were carried out on the innovative connectors assessed in [32], since their behaviour when subjected to shear was shown to be either independent of the connector material properties or solely dependent on the properties of the ordinary screws, but interaction tests were performed, as summarised below.

The second category of tests carried out previously [30, 34] was aimed at investigating the complex interactions between the three components of the composite system, namely the timber boards, the steel section and the connectors. The results of the interaction tests are presented in Table 2.

The interaction of the connector embedding into the timber was investigated by means of tests according to BS EN 383:2007 [39], carried out both on the screws [30] and the innovative connectors [32]. The expressions for the timber embedment strength f_h given in EN 1995-1-1 [40] are dependent on the connector diameter d, with the strength of bolted panel-to-timber connections being proportional to $d^{-0.6}$. The predictions resulting from this code expression [40] were in close agreement with the test results, with the latter indicating that the embedment strength is proportional to $d^{-0.5}$. For the innovative connectors, tests [34] have shown that the embedment interaction is essentially independent of the materials considered for the outer fitting.

Finally, the interaction of the screw head pulling-through the timber board was investigated, according to BS EN 1383 [41], while the interaction of the screw thread withdrawing through steel was examined in line with BS EN 1382 [42].

2.2. Push-out tests

The shear response of the connections, employing various screw orientations (i.e. perpendicular or diagonally to the board) [30] and different innovative connectors [32] was examined through push-out tests, carried out according to BS EN 26891 [43]. All particle board test results, including comparisons with ordinary self-drilling screws installed perpendicularly to the shear plane, are presented in Table 3. The labelling system adopted starts with the letter 'P' to indicate a push-out test and then specifies whether the thickness of the CFS section was 1.5 mm or 2.4 mm, using '15' or '24' respectively. For the ordinary screw tests described in [30], the next two numbers after the dash indicate the screw inclination in degrees measured from the normal to the shear plane, while the last letter, 'W' or 'N', indicates whether the screws were winged or non-winged. For the innovative shear connector tests described in [32], the letter 'P', 'S' or 'A' following the dash indicates whether the connector was made from plastic, steel or aluminium, while the last number specifies the connector type.

The obtained results [30] have shown that significant benefits in terms of stiffness can be gained when adopting inclined screws, with an increase in the slip modulus k_s (as defined in BS EN 26891 [43]) of up to 90% and 140% for the winged and non-winged screws respectively, and an increase in the mid-range slip modulus $k_{s,m}$ (measured between 40% and 70% of the estimated ultimate load) of up to 200% and 410% for the winged and non-winged screws respectively. Despite the achieved improvements in the slip modulus, it became evident during the preparation of the test specimens that the process of driving-in inclined screws was burdensome, with the screw tip prone to break during installation. Therefore, from a practical point of view, installation of inclined screws could overcomplicate and delay construction.

Tests on innovative connectors [32], bespoke to the flooring system being investigated, have shown that significant improvements in strength and slip modulus can be achieved with

connectors installed perpendicularly to the shear plane, if the formation of a plastic hinge within the connector is prevented and the embedment interaction is enhanced. Six connector types were investigated in [32]. Results have shown that Type 3 and Type 4 connectors, which include a self-locking mechanism, as shown in Figs. 2 and 3 respectively and described in Section 2.3, achieved significant improvements in slip moduli, with increases of up to 300% and 600% for k_s and $k_{s,m}$ respectively, when compared to the equivalent values achieved by ordinary self-drilling screws installed perpendicularly to the shear plane. Improvements in the ultimate load capacity were also achieved, with increases of up to 110% when compared to ordinary screws. From a practical perspective, specimen preparation has shown that these two types of connectors are relatively easy to install and, due to their integrated self-locking mechanism, no access is required from underneath the timber board. Note that Type 3 connectors can also be fully reused if the deformations experienced during the service life of the floor plate are within typical serviceability limits.

Following an assessment of all push-out tests carried out in [30] and [32], and considering both practicality of installation and performance, it was decided that two types of innovative connectors merit further investigation, Types 3 and 4; these were therefore employed in the composite beam tests described in Section 3.

2.3. Types of innovative connectors

In [32], six types of innovative connectors were explored, all of which required predrilling, were installed perpendicular to the shear plane and featured a 20 mm external diameter embedding into the timber board. It should be noted that only the connectors selected for further investigation, namely Types 3 and 4 as defined in Section 2.2, are described below.

The Type 3 connector, shown in Fig. 2, consists of a bevelled head, plastic outer fitting, with a diameter tapering from 20.1 mm towards the head end to 19.5 mm at the tail end, as shown in Fig. 4. The outer fitting also includes an 8 mm diameter hole, through which an 8 mm steel shank, including a 5 mm grade 10.9 bolt and a self-locking nut, is inserted. This connector required predrilling of an 8 mm and a 20 mm diameter hole in the steel sheet and timber board respectively. The connector is installed into the predrilled hole in the timber board with the steel shank, bolt and locking-nut protruding through the steel sheet. The bolt is then tightened from the top to mobilise the self-locking mechanism.

The Type 4 connector, shown in Fig. 3, has the same outer fitting dimensions (see Fig. 4) and requires the same predrilling in the timber board and steel sheet as Type 3, but, in this case, the fitting is made of aluminium and includes four tapered segments at the tail end. Upon tightening the bolt, the bevelled nut wedges itself into the four tapered segments, forcing them to open outwards and tighten against the steel sheet. Note that both the Type 3 and Type 4 connectors were tightened using a torque wrench, limiting the torque to 9 Nm for the conducted push-out tests [32].

3. Composite beam tests

Four-point bending tests were carried out to assess the flexural stiffness and moment capacity of the CFS-timber flooring system, featuring different shear connectors and connector configurations. Five composite beam specimens were tested in total, as described below.

3.1. Test specimens

All beam tests were carried out on specimens comprising 1.2 m wide by 38 mm thick wood-based floorboards and 300 mm deep and 1.5 mm thick CFS swage beams [33]. The nominal and average measured cross-sectional dimensions of the swage beam sections are presented in Fig. 5. For each test, two 4 m long swage beams were used. The beams were spaced 600 mm apart, as shown in Fig. 6. The overlying timber boards were placed symmetrically over the beams, as shown in Fig. 6(a). All connectors were installed perpendicularly to the shear plane. A summary of the test specimens is provided in Table 4. The arrangement of the screws described below seeks to limit the slip between the CFS beams and timber boards, which is largest toward the ends of the specimens.

The connectors employed for specimen No. 1, the benchmark test, were ordinary screws spaced at 300 mm, with the two central screws spaced at 150 mm on either side of the beam midspan. Specimen No. 2 was similar to No. 1, but with the last 3 screws at the end of each beam – within the length ‘E’ as shown in Fig. 6(a) – replaced by Type 3 innovative connectors. In specimen No. 3, the same length ‘E’ at the end of each beam contained 9 ordinary screws at 75 mm spacing. Specimen No. 4 included ordinary screws spaced at 75 mm throughout the length of the beam and wood adhesive along the joints of adjacent boards to ensure their immediate contact, minimising the effect of any gaps between the boards. The final composite beam test,

specimen No. 5, comprised a combination of ordinary screws, and Type 3 and Type 4 innovative connectors, spaced at 150 mm as shown in Fig. 7.

3.2. Experimental layout

The test setup, shown in Figs. 6 and 8, consisted of 4 m long specimens resting on rollers positioned at 100 mm from the beam ends, resulting in simply supported spans L of 3.8 m. The specimens were loaded at their third points, that is, at 1.267 m from the supports at either end, through a spreader beam which was loaded at its midspan by a 600 kN Holmatro hydraulic cylinder. The applied loads were measured by a 200 kN load cell [44]. As shown in Figs. 9(b) and 9(c), the CFS beams were stiffened at loading points and supports by a 150 mm length of the same beam cross-section, connected back-to-back. The stiffened sections also included timber infilling blocks and a timber diaphragm, all tied by a threaded bar linking the two main beams.

Three potentiometers on each beam were employed to measure vertical displacements, at the loading points and at midspan, while four further potentiometers, one at each end of each beam, were employed to measure the interface slip between the timber boards and the CFS sections. The interface slip measurements were achieved by installing the potentiometers on the underside of the timber boards with the tip resting on a steel bracket bolted directly to the beam. For specimens No. 3 to 5, two inclinometers per beam were also employed, installed on brackets placed at 0.5 m either side of the midspan and bolted to the mid-height of the beam web. Fig. 9 presents the full set of instrumentation used. Finally, five strain gauges were fixed on each beam section and another two at the top and bottom fibres of the timber boards at midspan, as shown in Fig. 9(d), to monitor the cross-sectional strain distribution.

Four loading and unloading cycles, with a 20 kN load increase in each subsequent cycle, were applied on each specimen, followed by loading up to failure, as shown in Fig. 10. This was performed to allow the measurement of any permanent deformation after each cycle. The setup was load controlled at a rate of 2 kN/min for the loading phases and 20 kN/min for the unloading and reloading phases (i.e. until the peak load of the previous cycle was reached). A period of 1 min of steady loading was maintained after each loading and unloading phase. All loads, displacements, strains and rotations were recorded at 0.5 s intervals, using the SignalExpress data acquisition software.

3.3. Specimen preparation observations

The key observations, challenges encountered and lessons learnt during the preparation of the tests specimens are reported in this section. It was evident during the specimen preparation that the size of the gap between the timber boards could have a direct impact on the effectiveness of the composite system. A wide gap would result in the adjacent timber boards not coming into contact during testing, thus leading to the beneficial effect of the compressive stress typically generated in the top component of a composite system being lost. This problem was mitigated by tightening each timber board against the one previously installed using long bar clamps. These clamps were held in place by a stopper secured to each side of the fixed board, as shown in Fig. 11. Note that this method of board tightening would be difficult to achieve in practice since access to both sides of the fixed timber board would be blocked by other boards of the flooring system. An alternative procedure that could be used in practice would be to temporarily fix stoppers to the timber board by means of screws, until the following board has been clamped and installed.

For the specimens with the innovative shear connectors, the predrilled holes required in the timber boards and the steel flanges were implemented by means of a pillar drill. However, in practice, holes in the timber boards could be predrilled as part of the manufacturing process, before being delivered on site. A customised drilling device, as shown in Fig. 12, having a smooth upper section fitting within the predrilled holes in the timber, and an 8 mm drill tip, could be used on site to ensure that the holes in the steel beam are aligned with the predrilled holes in the timber.

3.4. Results

The key results of the composite beam tests are presented in Table 5, where $P_{u,t}$ and $M_{u,t}$ are the maximum applied load and maximum moment per beam respectively, while $\delta_{u,t}$ and $s_{u,t}$ are the vertical displacement at midspan and the end slip at maximum load respectively. The average values for the two beams in each test are reported. It should be noted that the weights of the CFS beams, timber boards, spreader beam, loading sections, load cell, and of the stiffening setup described in Section 3.2, have been included in the calculation of the applied load and bending moments.

All specimens failed in-plane indicating that the floorboards and the connectors provided effective restraint against lateral torsional buckling. Specimens No. 1 to 3 failed by distortional buckling within the constant moment region, as shown in Figs. 13 and 14. On the other hand, specimens No. 4 and 5, which had a reduced connector spacing, failed primarily by local buckling with some distortional contribution. Local instability in these two specimens also occurred within the constant moment region as shown in Fig. 15.

The degree of restraint against vertical buckling displacements of the top flange is dependent on the thread withdrawal capacity and the connector spacing. It may be seen in Fig. 13, that the

top flange in specimen No. 1 withdrew from the screw thread. This shows that ordinary screws at 300 mm spacing did not effectively restrain the compressive flange against local/distortional buckling. Fig. 16, on the other hand, shows that when connectors at 150 mm spacing were employed, the compressive flange was effectively restrained. In this case, local buckling occurred adjacent to the connector position.

The effective flexural stiffness of the examined composite systems was determined based on the re-arranged formula for the elastic midspan displacement of a simply supported beam loaded at its third points:

$$(EI)_t = \frac{23PL^3}{648\delta_t} \ , \tag{1}$$

where P is the value of each point load applied at the beam thirds, L is the simply supported span and δ_t is the midspan displacement, taken as the average of the readings from the central potentiometers of both beams. Two stiffness values were calculated for each specimen: the initial effective stiffness $(EI)_{i,t}$, calculated at a load of around $0.2P_{u,t}$ and the mid-range effective stiffness $(EI)_{mid,t}$, calculated between $0.2P_{u,t}$ and $0.6P_{u,t}$ - see Table 5.

It should be mentioned that the effective flexural stiffnesses $(EI)_{i,t}$ and $(EI)_{mid,t}$ of the examined systems were also calculated based on the moment-curvature response in the uniform moment region of the beams, with the radius of curvature calculated either using the rotations recorded by the inclinometers or the vertical displacements at midspan and at points of load application. The values of stiffness calculated using the rotations were similar to those reported in Table 5, while significant discrepancies were observed for those yielded using the vertical displacements. This is attributed to the sensitivity of this calculation method to the differential movement between adjacent timber boards and the positions at which the displacement

measurements were taken (i.e. on the timber boards), with a tendency of the timber boards to bulge upwards, relative to the underlying steel beam, towards midspan.

The load - displacement (P_t - δ_t) curves and the load - average end slip (P_t - s_t) curves for all composite beam tests up to the ultimate load are plotted in Fig. 17 and Fig. 18 respectively. Note that the unloading cycles have been removed from the curves to ensure clarity of the results.

From Fig. 17 and Table 5, it can be observed that the introduction of Type 3 fittings at the beam ends in specimen No. 2 improved the ultimate load capacity and stiffness, compared to specimen No.1. Specimen No. 3 performed slightly better, with a higher initial stiffness and ultimate load. Specimens No. 4 and 5 displayed a similar load-displacement response, both performing better than all other specimens. Despite specimen No. 4 being initially the stiffest, it later exhibited a reduction in stiffness with increasing load, whilst specimen No. 5, which maintained a constant stiffness up to a load of around 40 kN per beam, had a stiffer response at higher loads, and reached the highest ultimate load.

The average end slip curves shown in Fig. 18 also indicate that specimens No. 2 and 5 performed better at higher load levels. Specimen No.2 displayed a steady rate of slip at higher loads, while specimen No. 5 displayed a reduction in the rate of slip at mid-range loads. All other specimens experienced an increase in the rate of slip, hence a decrease in stiffness, as the loads increased. It should be noted that although specimens No. 3 and 4 displayed an almost identical load-average end slip response, a proportion of slip in the third specimen would have been dissipated at each board joint until the gaps are closed and boards are in full contact; hence, this proportion of the slip was not captured by the potentiometers. Gaps at the board joints were eliminated in the final two specimens by the addition of glue. Therefore, whereas the end slip in specimens No. 4 and 5 is reflective of the total interface slip resulting from half

of the composite beam (from midspan to the beam ends), that measured for the other three specimens that had no glue at the joints, would need to be increased by the summation of gaps between the boards.

The strain distributions at $0.5P_{u,t}$ and $P_{u,t}$, measured by the strain gauges fixed to the CFS beam and timber boards at midspan, are shown in Fig. 19. It can be seen that the neutral axis shifts upwards with increasing load. This is attributed to the closure of gaps between the boards, increasing their effectiveness in transferring compressive stresses. The significant shift that occurred in specimen No. 5 is also attributed to the increased effectiveness of the innovative connectors at higher slips, leading to an enhanced degree of shear connection - see Section 4.3.

The average permanent midspan deformations after each load cycle for all beam specimens were very similar, as shown in Fig. 20, increasing by about 0.5 mm after each load cycle.

4. Analysis of results

4.1. Flexural stiffness of CFS-timber composite beams

The flexural stiffness of composite beams is directly related to the stiffness of the shear connection at the interface between the system components. If the components are not connected and can thus slip relative to each other, they act independently, with their individual cross-sectional properties, including their individual flexural stiffness, activated when subjected to bending moments. On the other hand, if the relative slip at the interface is fully restrained, the two components have full interaction and act monolithically, having a composite cross-section, with its properties influenced by the two different Young's moduli. Achieving full interaction in practice is unrealistic, since an infinitely stiff connection would be required to fully restrain the slip between the individual components.

Note that a distinction must be made between the concepts of full interaction and full shear connection, with the former term being related to the stiffness of the shear connection, and implying no relative slip between the components, and the latter being related to the strength of the shear connection, referring to a system with connectors capable of transferring the shear forces that develop when the full plastic moment capacity of the system is attained. Hence, while a system with full interaction cannot be realised in practice, one with full shear connection is achievable.

4.1.1. Determination of the theoretical effective flexural stiffness

A method for determining the effective flexural stiffness of mechanically jointed timber beams is presented in Section B.2 of Annex B of EN 1995-1-1 [40]. This approach is based on the gamma method, first proposed by Möhler [45], with its full derivation presented by Kreuzinger

[46]. The model has been effectively adapted to timber-concrete [47-49] and, more recently, to timber-CFS composite systems [8, 12]. In this section, the approach introduced in [8] for beams similar to those examined herein has been extended to allow for varying connector stiffness and spacing.

Consider a simply supported composite beam of span L, as shown in Fig. 21, consisting of a CFS section of area A_s, second moment of area I_s, Young's modulus E_s and depth h, mechanically connected to overlying timber boards of area A_t, second moment of area I_t, Young's modulus E_t and thickness t. The connectors are installed at a spacing s and have a slip modulus K.

When the beam is subjected to a vertical load, it deforms as shown in Fig. 22, and the relative slip at the beam-board interface is restricted by the connectors, which consequently develop an internal shear force F_{con}. With reference to the internal forces acting on an incremental portion of the composite beam of length dx, the equilibrium equations for the axial and shear forces and bending moments lead to Eq. 2 [8] for the calculation of the effective flexural stiffness $(EI)_{eff}$ of the composite system:

$$(EI)_{eff} = E_t I_t + E_s I_s + \frac{E_t A_t \gamma \alpha^2}{1 + \gamma \frac{E_t A_t}{E_s A_s}} \tag{2}$$

where:

$$\alpha = \frac{t + h}{2} \tag{3}$$

and γ is the shear bond coefficient, given by:

$$\gamma = \frac{1}{1 + \frac{\pi^2}{L^2} \frac{E_t A_t}{k}} \tag{4}$$

In Eq. 4, k is the smeared slip modulus at the interface, related to the slip modulus of each connector K by:

$$k = \frac{K}{s} \tag{5}$$

Note that although this solution has been derived assuming a sinusoidally distributed load (thus resulting in a sinusoidal bending moment diagram), it has been shown that it is also reasonably accurate and applicable to most other load distributions [46, 48].

It should be noted that the span L considered in Eq. 4, should be taken equal to the summation of the critical lengths of the composite beam (i.e. those lengths experiencing a shear force). For instance, considering the beams presented in Section 3 subjected to four-point bending, the length input into Eq. 4 should be equal to two-thirds of the simply supported span, which is equal to the summation of the two (outer) portions of the beam experiencing a variation in bending moment and, hence, a shear force.

Generally, slip values increase when moving away from the beam midspan, however, slip measurements in [8] have shown that within the critical lengths, slip values are approximately constant, particularly for connector spacings less than 160 mm. Therefore, in situations where different groups of connectors are employed within the critical lengths of a beam with their slip moduli varying, the average slip modulus K_{avg} given by Eq. 6 can be used in Eq. 5 in place of K:

$$K_{avg} = \frac{\sum K_i n_i}{\sum n_i} \tag{6}$$

where K_i is the slip modulus of a connector from group i and n_i is the number of connectors in group i, with each group comprising connectors with the same slip modulus.

If, on the other hand, the spacing of the connectors varies, then the average smeared slip modulus k_{avg} should be used in Eq. 4 in place of k:

$$k_{avg} = \frac{Kn}{L} \tag{7}$$

where n is the quantity of connectors within the critical length L.

If both the spacing and the slip moduli of the connectors are varying, the average slip modulus is first found using Eq. 6 and the resulting value is then used in Eq. 7 to find the average smeared slip modulus.

4.1.2. Flexural stiffness of composite beams assuming full interaction

The flexural stiffness of a composite system assuming full shear interaction, although not practically achievable, provides an upper bound limit against which the experimental values achieved in this study can be compared. The flexural stiffness of a composite system with full shear interaction is given by:

$$(EI)_{comp} = E_t I_t + E_s I_s + E_t A_t \left(y_{comp} - [h + y_t]\right)^2 + E_s A_s \left(y_{comp} - y_s\right)^2 \tag{8}$$

where y_{comp} is the distance from the centroid of the fully composite section to its base, while y_t and y_s are the distances from the centroid to the base of the timber board and steel section respectively, as shown in Fig. 23.

4.1.3. Comparison of experimental results with theoretical flexural stiffness values

Table 6 presents comparisons between the values of the effective flexural stiffness $(EI)_{eff}$ determined using the method presented in Section 4.1.1 and those obtained from the beam tests

$(EI)_{i,t}$. Additional experimental flexural stiffness data reported in the literature [50] and [51] for simply supported composite beams with 250 mm deep swage beams and 254 mm deep lipped channel sections, have also been included in the presented comparisons. A summary of the test specimens examined in [50] and [51] is included in Table 7.

The comparisons presented in Table 6 show that the proposed method can accurately predict the effective flexural stiffness of the examined composite systems, with an average $(EI)_{eff}$ / $(EI)_{i,t}$ ratio of 0.93 and an associated coefficient of variation of 0.14. The validity of the proposed extension of the method to cater for irregular connector spacing and varying slip moduli is therefore demonstrated. Values of the flexural stiffness of the bare steel section $(EI)_{bare}$ and of the composite section assuming full interaction $(EI)_{comp}$ have also been presented in Table 6, defining the lower and upper bound values for each composite beam configuration.

4.2. Moment capacity of CFS-timber composite beams

The beneficial influence of composite action on the moment capacity of composite beams depends on the degree of shear connection at the interface between the system components. A design method devised in [8] for the determination of the degree of shear connection and, hence of the moment capacity of CFS-timber composite systems has been appropriately adapted and applied to the specimens examined herein. A summary of the method, as well as its validation against the obtained test data, is presented in this section.

4.2.1. Moment capacity of a fully composite system

In a fully composite system the moment capacity of the section is governed either by the strength of the steel section or that of the timber boards, whichever is the weakest. Therefore, with reference to Fig. 24, the force to be transferred by the connectors in a system with full shear connection V is limited either by the compressive strength of the timber boards $F_{c,t}$ or by the tensile strength of the CFS section $F_{t,s}$:

$$V = min\left(F_{c,t}; F_{t,s}\right) \tag{9}$$

with:

$$F_{c,t} = A_t \frac{f_{c,t}}{\gamma_M} \tag{10}$$

$$F_{t,s} = A_s \frac{f_y}{\gamma_{M0}} \tag{11}$$

where $f_{c,t}$ is the compressive strength of the timber board material, f_y is the yield strength of the CFS beam while γ_M and γ_{M0} are the material partial safety factors for timber [40] and steel [52] respectively. It should be noted that for the systems examined herein, consisting of beams spaced at 600 mm, physical tests [10] and numerical simulations [14] have shown that there is no evidence of shear lag across the width of the board and, therefore, the width considered when calculating A_t was taken as equal to the spacing of the beams. Further investigation is required for beam spacings exceeding 600 mm.

The number of shear connectors required per critical length, as defined in [53], for a fully composite system n_f can be determined from Eq. 12, where F_v is the shear force that can be withstood by each connector and may either be determined from push-out test data or using the methodology presented in [32] and [34].

$$n_f = \frac{V}{F_v} \tag{12}$$

Assuming full plastic redistribution, EN 1994-1-1 [53] allows ductile connectors to be uniformly spaced along that critical length. Hence, a simply supported composite beam subjected to a uniform load, which has two identical critical lengths, each from mid-span to one of the supports, requires a total of $2n_f$ connectors for a fully composite system and these may be spread uniformly along the beam.

As described in [8] and with reference to Fig. 24, the plastic moment capacity $M_{pl,comp}$ of a fully composite system can be determined based on cross-sectional equilibrium. The derived formulae [8] depend on the position of the plastic neutral axis (PNA), which can be located within the timber board, within the CFS beam or at their interface.

Note that CFS sections are typically classified as Class 3 or Class 4 and, thus, have their moment resistance limited to either the elastic or the effective moment capacity due to local instabilities. However, for a composite system with full shear connection, the compression flange of the CFS section is restrained by the overlying board, while a reduced extent of the CFS web is under compression due to the upward shift of the neutral axis. Under such circumstances, particularly when the compressive capacity of the timber board is comparable to, or exceeds, the tensile capacity of the steel section, $M_{pl,comp}$ may be attained.

4.2.2. Moment capacity of a composite system with partial shear connection

When the total strength of the shear connectors provided within a critical length is less than that required to develop full shear connection (i.e. lower than the result given by Eq. 9), then the shear connection is partial. Therefore, the moment capacity of a composite section with partial shear connection is governed by the strength of the shear connection. The degree of

shear connection η_d, for a system consisting of n connectors of the same properties per critical length, is given by:

$$\eta_d = \frac{n}{n_f} \leq 1 \tag{13}$$

If the connectors are not the same, then Eq. 13 may be rewritten as:

$$\eta_d = \frac{\sum F_{v,i}}{V} \leq 1 \tag{14}$$

where $F_{v,i}$ is the shear strength of the i^{th} connector.

An extension of the EN 1994-1-1 [53] design approach for determining the moment capacity of composite steel-concrete systems comprising Class 1 or 2 steel sections with partial shear connection to CFS-timber systems with Class 3 or 4 sections was introduced in [8]. As shown in Fig. 25, this approach [8] can be used to determine the moment capacity of a CFS-timber composite system based either on plastic theory:

$$M_{c,Rd} = M_{pl,Rd} - (1 - \eta_d)\left(M_{pl,bare} - M_{bare}\right) \tag{15}$$

or a more conservative simplified linear expression:

$$M_{c,lin,Rd} = M_{bare} + \eta_d\left(M_{pl,comp} - M_{bare}\right) \tag{16}$$

where $M_{pl,Rd}$ and $M_{pl,bare}$ are the plastic moment capacities of the composite system with partial shear connection and the bare steel section respectively, while M_{bare} is the elastic or the effective moment capacity (depending on the classification of the cross-section) of the bare steel section.

Note that, in line with the recommendations set out in [8], when $\eta_d < 0.05$, no composite action should be considered, and the moment capacity of the system should be limited to that of the bare steel section M_{bare}. Also note that for a Class 4 section, the effective cross-section to be

considered for the calculation of the effective moment capacity may be determined according to EN 1993-1-3 [54] and EN 1993-1-5 [55].

4.2.3. Comparison of predicted moment capacities with experimental results

Comparisons between the moment capacities predicted by the method described in Section 4.2.2 (for both the linear approach $M_{c,lin,Rd}$ and the plastic theory approach $M_{c,Rd}$) and the experimental results $M_{u,t}$ are presented in Table 8. Note that the experimental data reported in [50] and [51], a summary of which is presented in Table 7, have also been included in the comparisons. The values of the degree of shear connection η_d, of all specimens, as well as the moment capacities M_{bare}, $M_{pl,bare}$, and $M_{pl,comp}$, which are required for the calculation of the predicted moment capacities of the composite systems, are also reported in Table 8. The comparisons confirm that the approach based on the plastic theory is more accurate than the simplified linear expression, with average prediction-to-test ratios equal to 0.91 and 0.83 respectively, and a coefficient of variation equal to 0.09 and 0.12 respectively.

4.3. Performance of innovative shear connectors in composite beam systems

It is evident from Table 6 that for the specimens with the innovative shear connectors (i.e. specimens No. 2 and No. 5), the initial stiffness determined from the experiments was lower, by 8% on average, than that predicted by the method presented in Section 4.1.1. In Fig. 17, it can be observed that the stiffness of these composite specimens improved with increasing loads; a similar trend is also evident in Fig. 18, as noted in Section 3.4.

The lower initial stiffnesses are attributed to the initial tolerance gaps between the different connector components. From Fig. 18, it can be seen that there was very little slip in the initial stages of loading, generally less than 0.5 mm end slip for loads up to around 50% of the

ultimate. This means that even the slightest tolerance gaps had a significant impact on the initial stiffness of the system. It is only when the generated slip is sufficient to bring all the individual components into direct contact that the connector can be deemed to be fully effective. Since slip is dependent on the span of the beam, it can be assumed that the performance of the connectors would improve for longer spans, but further investigation would be required for this to be confirmed.

5. Conclusions

An experimental investigation into the structural response of CFS-timber composite flooring systems, featuring a combination of ordinary self-drilling screws [30] and innovative shear connectors [32], has been presented. It has been shown that the performance of the innovative connectors improves with increasing load, with this trend being attributed to the closure of tolerance gaps between the various connector components as the interface slip increases. The best performing specimen, comprising a combination of ordinary screws and innovative connectors at 150 mm spacing, achieved increases of up to about 45% in moment capacity and almost 20% in mid-range stiffness, when compared to the benchmark specimen with ordinary screws at 300 mm spacing.

The applicability of design methods reported in the literature for the calculation of the effective flexural stiffness and moment capacity of CFS-timber composite systems has been evaluated by comparisons against the obtained experimental data. In addition, these methods have been adapted to cater for varying screw spacings and varying connector strengths, and it has been shown that accurate predictions of the effective stiffness and moment capacity of the examined systems can be achieved, with mean prediction-to-test ratios of 0.93 and 0.91 respectively.

Acknowledgements

The research work in this experimental programme was partially funded by the ENDEAVOUR Scholarships Scheme. The authors would like to thank Ayrshire Metal Products for supplying the testing material and EMPAV Ltd. for machining the connectors required for the experimental program.

References

[1] Kelly, A. and Zweben, C., '*Comprehensive Composite Materials*'. Elsevier, Pergamon press, 2000.

[2] Hassanieh, A., Valipour, H.R. and Bradford, M.A., '*Load-slip behaviour of steel-cross laminated timber (CLT) composite connections*'. Journal of Constructional Steel Research, 2016, Vol. 122: 110-121.

[3] Hassanieh, A., Valipour, H.R. and Bradford, M.A., '*Experimental and analytical behaviour of steel-timber composite connections*'. Construction and Building Materials, 2016, Vol. 118: 63-75.

[4] Sheta, A., Ma, X., Zhuge, Y., ElGawady, M., Mills, J. and Abd-Elaal, E., '*Flexural strength of innovative thin-walled composite cold-formed steel/PE-ECC beams*'. Engineering Structures, 2022, Vol. 267: 114675.

[5] Cicione, A. and Walls, R., '*The effect of shear connectors on the strength, serviceability and dynamic response of composite floors using cold-formed steel beams and concrete in decking*'. Engineering Structures, 2022, Vol. 269: 114806.

[6] Hosseinpour, M., Zeynalian, M., Ataei, A. and Daei, M., '*Push-out tests on bolted shear connectors in composite cold-formed steel beams*'. Thin-Walled Structures, 2021, Vol. 164: 107831.

[7] Navaratnam, S., Widdowfield Small, D., Gatheeshgar, P., Poologanathan, K., Thamboo, J., Higgins, C. and Mendis, P., '*Development of cross laminated timber-cold-formed steel composite beam for floor system to sustainable modular building construction*'. Structures, 2021, Vol. 32: 681-690.

[8] Kyvelou, P., Gardner, L. and Nethercot, D.A., '*Design of Composite Cold-Formed Steel Flooring Systems*'. Structures, 2017, Vol. 12: 242-252.

[9] Kyvelou, P., Gardner, L. and Nethercot, D.A., '*Composite Action Between Cold-Formed Steel Beams and Wood-Based Floorboards*'. International Journal of Structural Stability and Dynamics, 2015, Vol. 15(8):1540029 (17 pp.).

[10] Kyvelou, P., Gardner, L. and Nethercot, D.A., '*Testing and Analysis of Composite Cold-Formed Steel and Wood-Based Flooring Systems*'. Journal of Structural Engineering, 2017, Vol. 143(11): 04017146.

[11] Gandomkar, F.A., Wan Badaruzzaman, W.H., Osman, S.A. and Ismail, A., '*Experimental and numerical investigation of the natural frequencies of the composite profiled steel sheet*

dry board (PSSDB) system'. Journal of the South African Institution of Civil Engineering, 2013, Vol. 55 No.1 Paper 783: 11-21.

[12] Kyvelou, P., Reynolds, T.P.S., Beckett, T.S.C. and Huang, Y., '*Experimental investigation on composite panels of cold-formed steel and timber*'. Engineering Structures, 2021, Vol. 247: 113186.

[13] Shi, Y., Yang, K., Guan, Y., Yao, X., Xu, L. and Zhang, H., '*The flexural behaviour of cold-formed steel composite beams*'. Engineering Structures, 2020, Vol. 218: 110819.

[14] Kyvelou, P., Gardner, L. and Nethercot, D.A., '*Finite Element Modelling of Composite Cold-Formed Steel Flooring Systems*'. Engineering Structures, 2018, Vol. 158: 28-42.

[15] Bejtka, I. and Blass, H.J., '*Joints with Inclined Screws*'. Proceedings, CIB-W18 Timber Structures, Meeting 35, Paper 35-7-4, 2002.

[16] Kevarinmäki, A., '*Joints with Inclined Screws*'. Proceedings, CIB-W18 Timber Structures, Meeting 35, Paper 35-7-3, 2002.

[17] Tomasi, R., Crosatti, A. and Piazza, M., '*Theoretical and experimental analysis of timber-to-timber joints connected with inclined screws*'. Construction and Building Materials, 2010, Vol. 24: 1560-1571.

[18] Jockwer, R., Steiger, R. and Frangi, A., '*Design Model for Inclined Screws Under Varying Load to Grain Angles*'. Proceedings, International Network on Timber Engineering Research, Meeting 47, Paper 47-7-5, 2014.

[19] Girhammar, U.A., Jacquier, N. and Källsner, B., '*Stiffness model for inclined screws in shear-tension mode in timber-to-timber joints*'. Engineering Structures, 2017, Vol. 136: 580-595.

[20] Jacquier, N. and Girhammar, U.A., '*Tests on glulam-CLT shear connections with double-sided punched metal plate fasteners and inclined screws*'. Construction and Building Materials, 2014, Vol. 72: 444-457.

[21] Jacquier, N., 'Development and Evaluation of Mechanical Joints for Composite Floor Elements with Cross Laminated Timber'. PhD Thesis. Lulea University of Technology. 2015.

[22] Jacquier, N. and Girhammar, U.A., '*Evaluation of bending tests on composite glulam-CLT beams connected with double-sided punched metal plates and inclined screws*'. Construction and Building Materials, 2015, Vol. 95: 762-773.

[23] Meierhofer, U., '*A Timber/Concrete Composite System*'. Structural Engineering International, 1993, Vol. 3(2): 104-107.

[24] Steinberg, E., Selle, R. and Faust, T., '*Connectors for Timber-Lightweight Concrete Composite Structures*'. Journal of Structural Engineering, 2003, Vol. 129(11), 1538-1545.

[25] Kavaliauskas, S., Kvedaras, A.K. and Valiūnas, B., '*Mechanical Behaviour of Timber-to-Concrete Connections with Inclined Screws*'. Journal of Civil Engineering and Management, 2007, Vol. 13(3), 193-199.

[26] Kavaliauskas, S., and Kvedaras, A.K., '*The Predictive Model for Load-Carrying Capacity of Inclined Screws as Connecting-Links in Timber-Concrete Composite Beams*'. 10th International Conference – Modern Building Materials, Structures and Techniques, 2010, 683-690.

[27] Symons, D., Persaud, R. and Stanislaus, H., '*Slip Modulus of Inclined Screws in Timber-Concrete Floors*'. Proceedings, Institution of Civil Engineers – Structures and Buildings, 2010, Vol.163(4): 245-255.

[28] Khorsandnia, N., Valipour, H.R. and Crews, K., '*Experimental and analytical investigation of short-term behaviour of LVL-concrete composite connections and beams*'. Construction and Building Materials, 2012, Vol. 37: 229-238.

[29] Moshiri, F., Gerber, C., Valipour, H.R., Shrestha, R. and Crews, K.I., '*The predictive model for strength of inclined screws as shear connection in timber-concrete composite floor*'. Proceedings, Conference on the Mechanics of Structures and Materials, 2013, pp. 1059-1064.

[30] Vella, N., Gardner, L. and Buhagiar, S., '*Experimental analysis of cold-formed steel-to-timber connections with inclined screws'*. Structures, 2020, 24:890-904.

[31] Kyvelou, P., Nethercot, D.A., Hadjipantelis, N., Kyprianou, C. and Gardner, L., '*The evolving basis for the design of light gauge steel systems*'. International Journal of Structural Stability and Dynamics, 2020, Vol. 20, No. 13: 2041008.

[32] Vella, N., Kyvelou, P., Buhagiar, S. and Gardner, L., '*Innovative shear connectors for composite cold-formed steel-timber structures: an experimental investigation*'. Engineering Structures, 2023, Vol. 287: 116120.

[33] Ayrshire Metals Limited. Product Brochure. Available from: https://www.ayrshire.co.uk/_files/ugd/e0b978_7b9f1a5575784a699110abcc12ce68a2.pdf [Accessed December 2022].

[34] Vella, N., Gardner, L. and Buhagiar, S., '*Analytical modelling of cold-formed steel-to-timber connections with inclined screws'*. Engineering Structures, 2021, Vol. 249: 113187.

[35] EN 789, '*Timber structures – Test methods – Determination of mechanical properties of wood based panels*'. Brussels, European Committee for Standardization, 2004.

[36] EN ISO 6892-1, '*Metallic materials – Tensile testing. Part 1: Method of test at room temperature*'. Brussels, European Committee for Standardization, 2016.

[37] EN ISO 898-1, '*Mechanical properties of fasteners made of carbon steel and alloy steel*'. Brussels, European Committee for Standardization, 2013.

[38] ASTM Standard F1575, '*Standard Test Method for Determining Bending Yield Moment of Nails*'. ASTM International, West Conshohocken, PA, 2017.

[39] EN 383, '*Timber structures – Test methods – Determination of embedment strength and foundation values for dowel type fasteners*'. Brussels, European Committee for Standardization, 2007.

[40] EN 1995-1-1. Eurocode 5: '*Design of timber structures. Part 1-1: General – Common rules and rules for buildings'*. European Committee for Standardisation, Brussels, 2004.

[41] EN 1383, '*Timber structures – Test methods – Pull through resistance of timber fasteners*'. Brussels, European Committee for Standardization, 2016.

[42] EN 1382, '*Timber structures – Test methods – Withdrawal capacity of timber fasteners*'. Brussels, European Committee for Standardization, 2016.

[43] EN 26891, '*Timber structures – Joints made with mechanical fasteners – General principles for the determination of strength and deformation characteristics*'. Brussels, European Committee for Standardization, 1991.

[44] Tokyo Measuring Instruments Lab – Centre-hole type compression load cell. Specs. Available from: https://www.tml.jp/eng/documents/transducers/CLC-NA.pdf [Accessed December 2022].

[45] Möhler, K., '*Über das Tragverhalten von Biegeträgern und Druckstäben mit zusammengesetztem Querschnitt und nachgiebigen Verbindungsmitteln*'. Habilitation, 1956, TH Karlsruhe.

[46] Kreuzinger, H., '*Mechanically jointed beams and columns*', in: Blass H.J., Aune, P., Choo, B.S., Görlacher, R., Griffiths, D.R., Hilson, B.O., Racher, P. and Steck, G., Timber Engineering. STEP 1. Basis of design, material properties, structural components and joints. Centrum Hout, The Netherlands, 1995, pp. B11/1-8.

[47] Van der Linden, M.L.R., '*Timber-concrete composite floor systems*'. PhD Thesis. TU Delft. 1999.

[48] Nežerka, V., '*Timber-concrete composite structures*'. Bachelor Thesis. Czech Technical University in Prague. 2010.

[49] Mauro, D. and Marcelo, T., '*Semirigid composite wood-concrete T-Beams*'. Proceedings of World Conference on Timber Engineering, P47, British Columbia, Canada, 2000.

[50] Kyvelou, P., '*Structural Behaviour of Composite Cold-Formed Steel Systems*'. PhD Thesis. Imperial College London. 2017.

[51] Karki, D., '*Numerical and Experimental Investigations on Static Behaviour of Composite Cold-Formed Steel and Timber Flooring System*'. PhD Thesis. University of Technology Sydney. 2023.

[52] EN 1993-1-1. Eurocode 3: '*Design of steel structures. Part 1-1: General rules and rules for buildings'*. European Committee for Standardisation, Brussels, 2005.

[53] EN 1994-1-1. Eurocode 4: '*Design of composite steel and concrete structures. Part 1-1: General rules and rules for buildings'*. European Committee for Standardisation, Brussels, 2004.

[54] EN 1993-1-3. Eurocode 3: '*Design of steel structures. Part 1-3: General rules – Supplementary rules for cold-formed members and sheeting'*. European Committee for Standardisation, Brussels, 2006.

[55] EN 1993-1-5. Eurocode 3: '*Design of steel structures. Part 1-5: Plated structural elements'*. European Committee for Standardisation, Brussels, 2006.

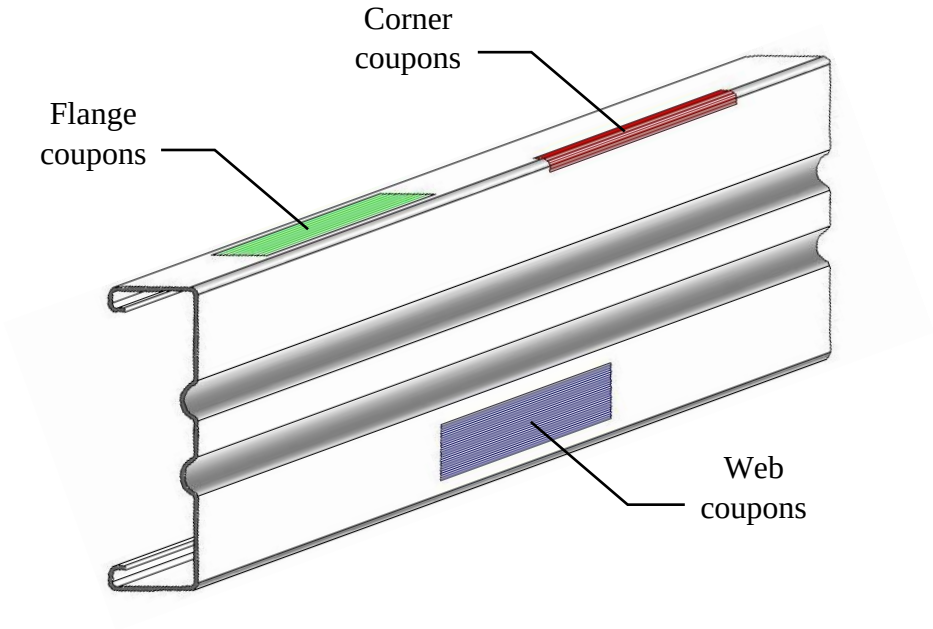

Fig. 1. Locations of extraction of CFS tensile coupons [30]

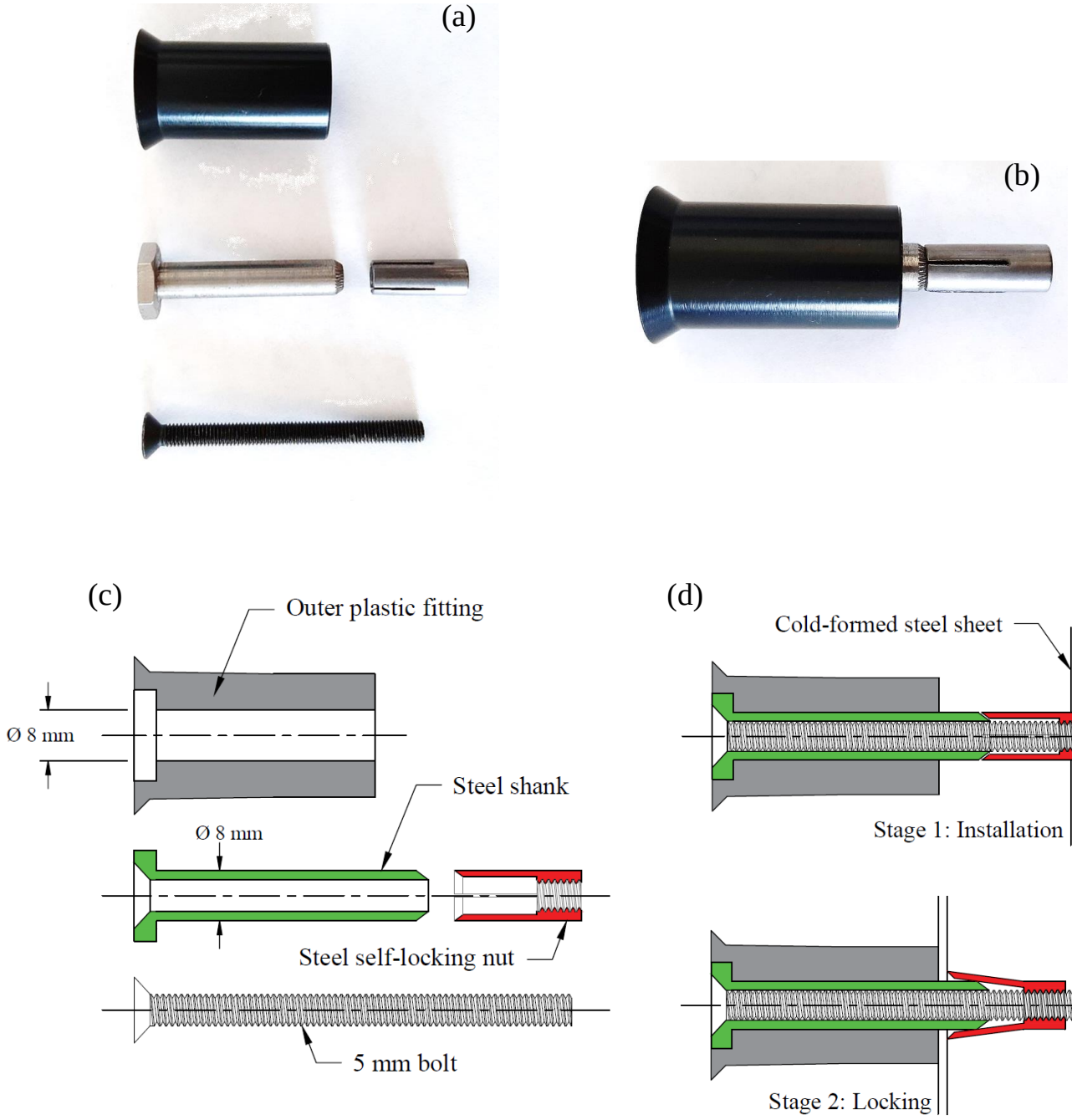

Fig. 2. Type 3 connector (a) Dismantled, (b) Assembled, (c) Cross-sectional details, (d) Assembly detail [32]

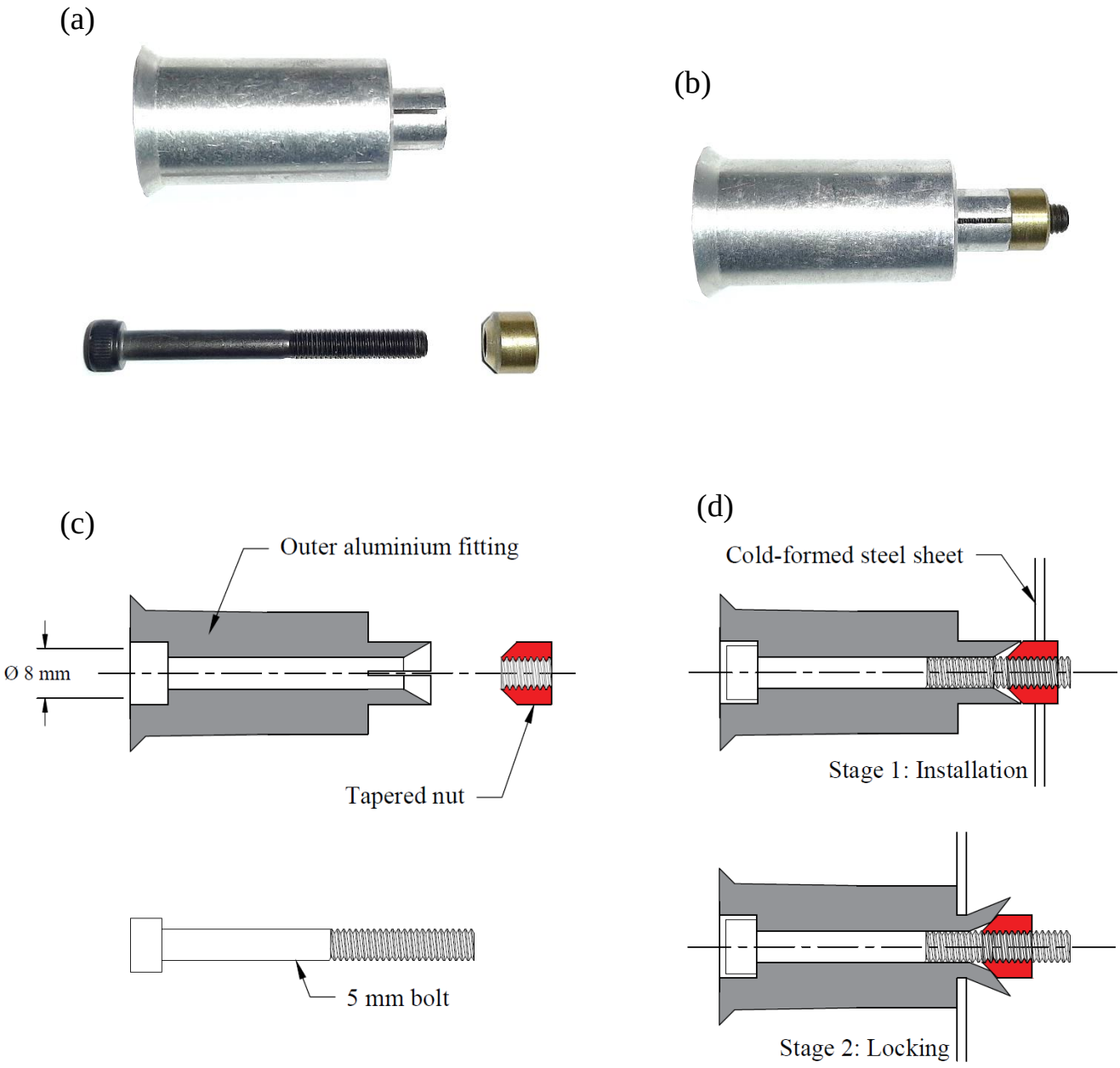

Fig. 3. Type 4 connector: (a) Dismantled, (b) Assembled, (c) Cross-sectional details, (d) Assembly detail [32]

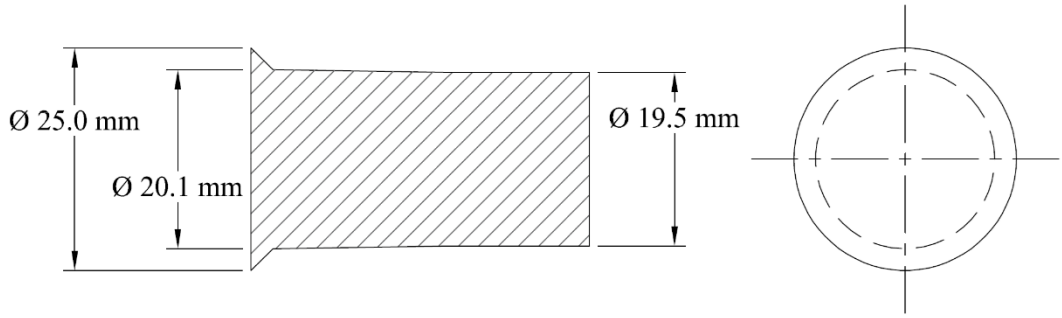

Fig. 4. Outer fitting dimensions of innovative connectors [32]

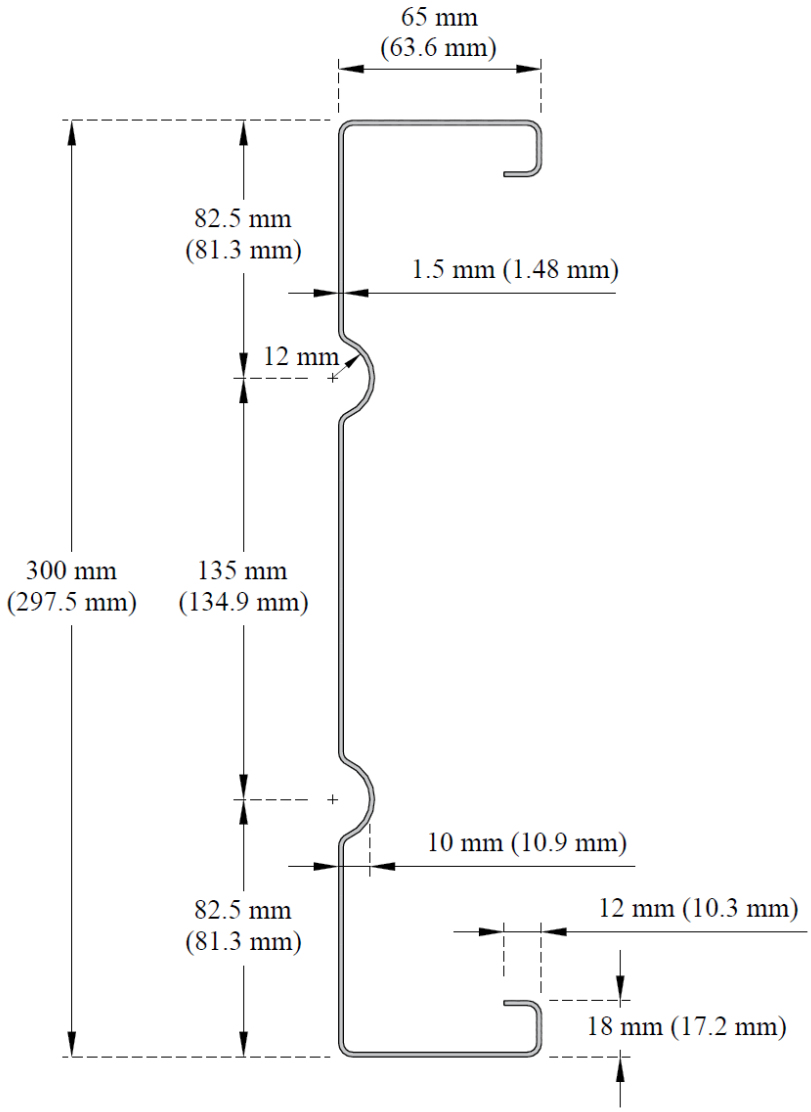

Fig. 5. Nominal and average measured (in brackets) cross-sectional dimensions of 300 mm deep swage beam [33]

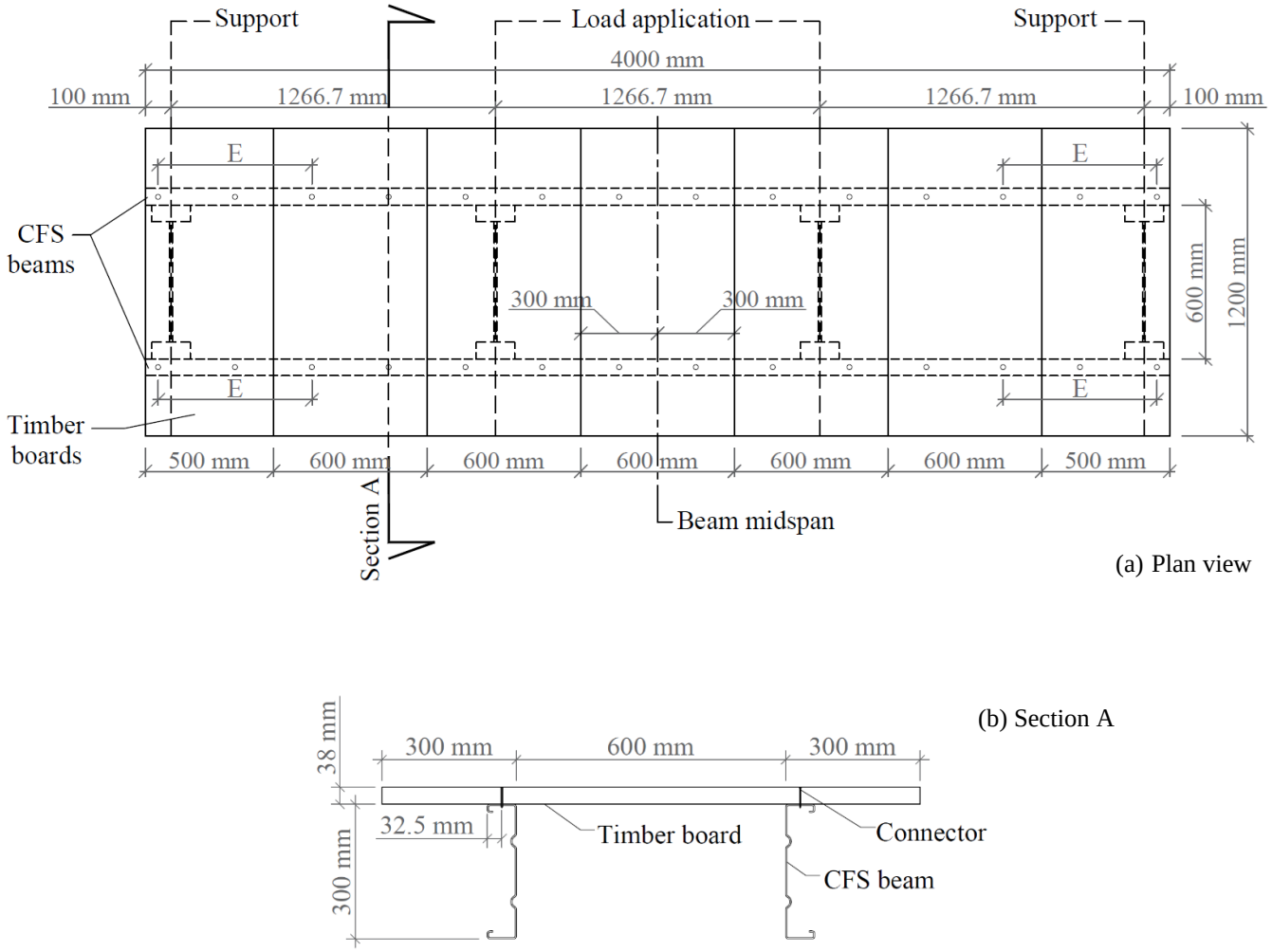

Fig. 6. Composite beam specimen details – (a) Plan view, (b) Section A

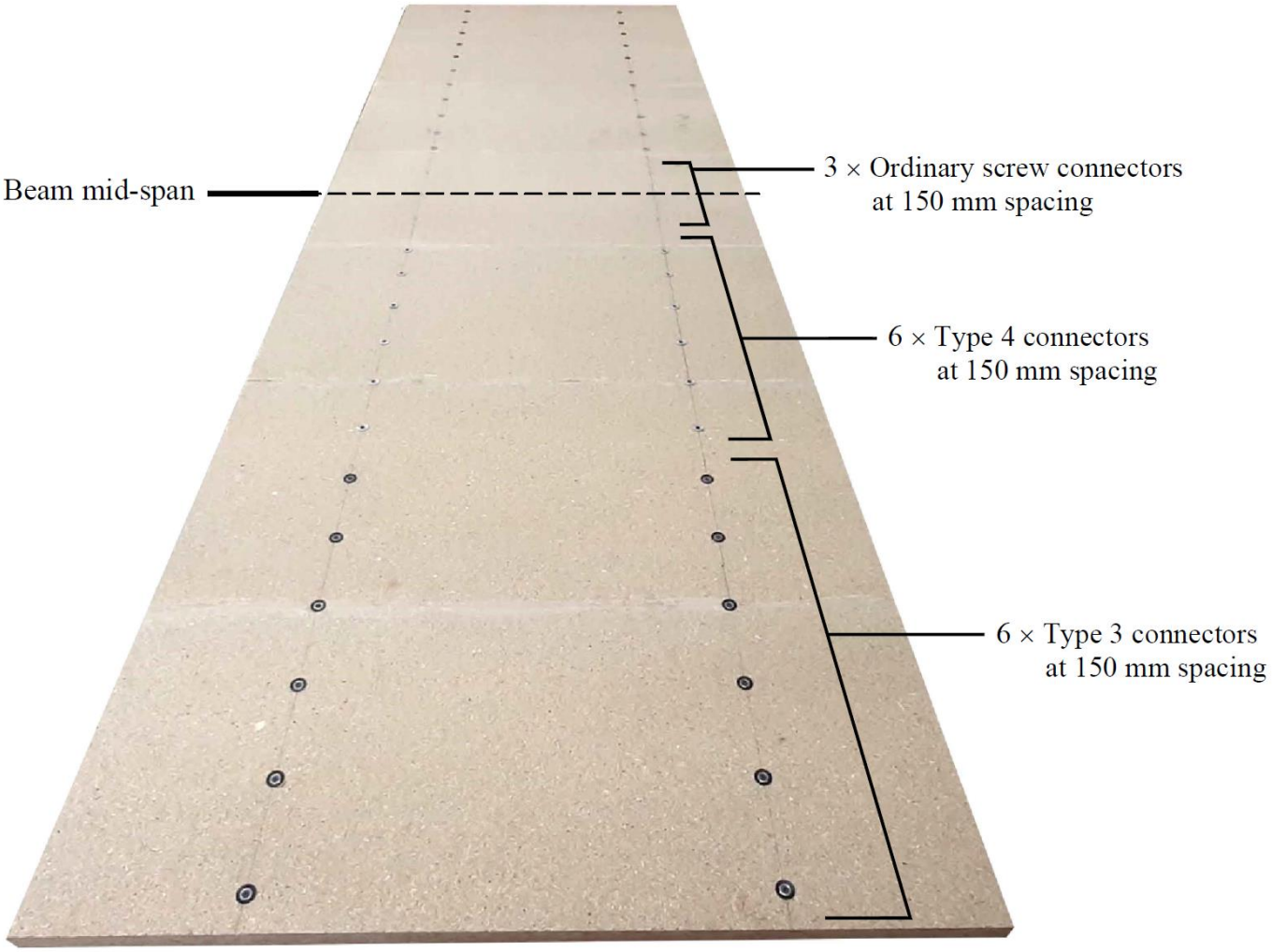

Fig. 7. Specimen No. 5 – connector configuration

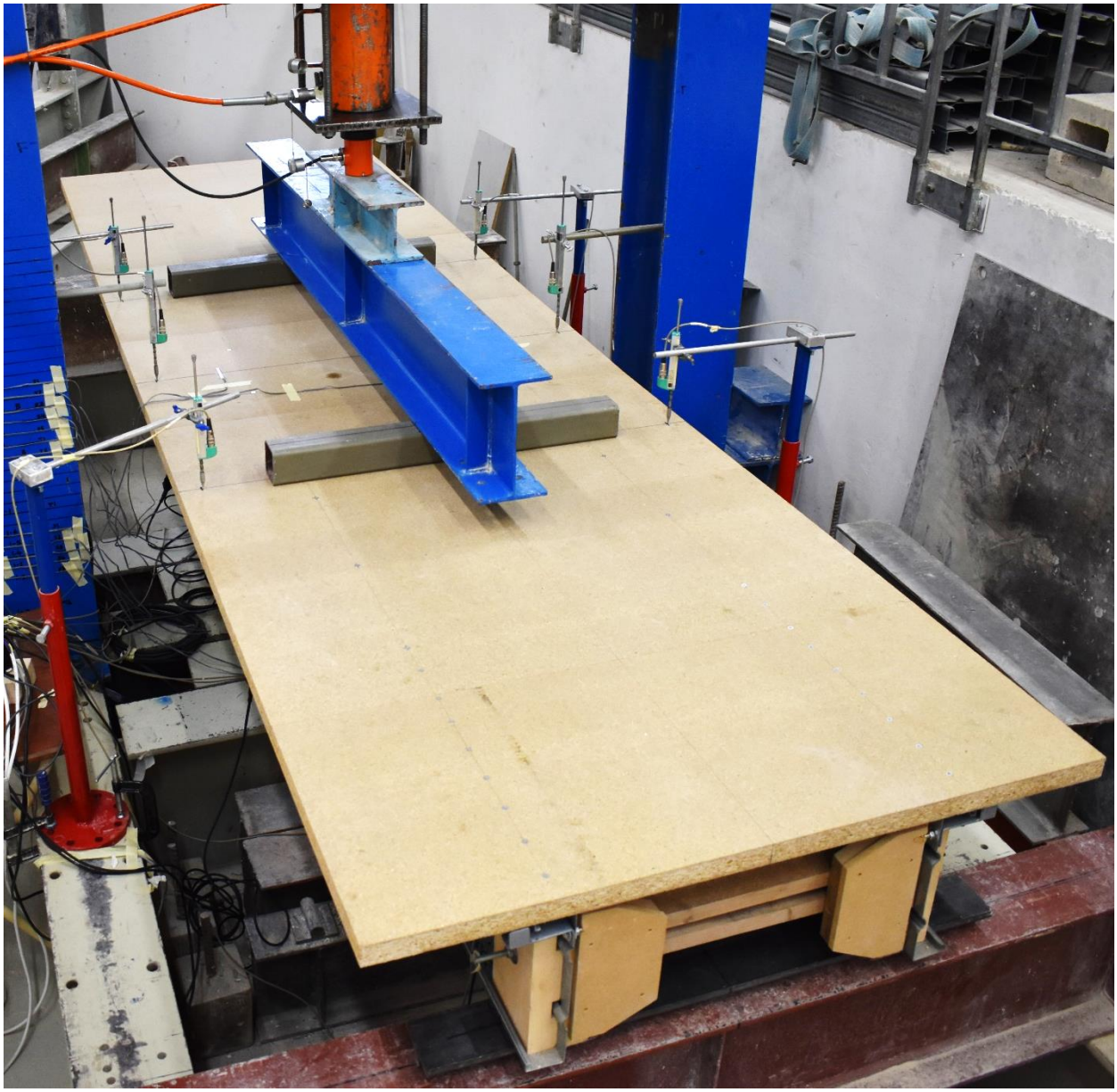

Fig. 8. Composite beam test setup

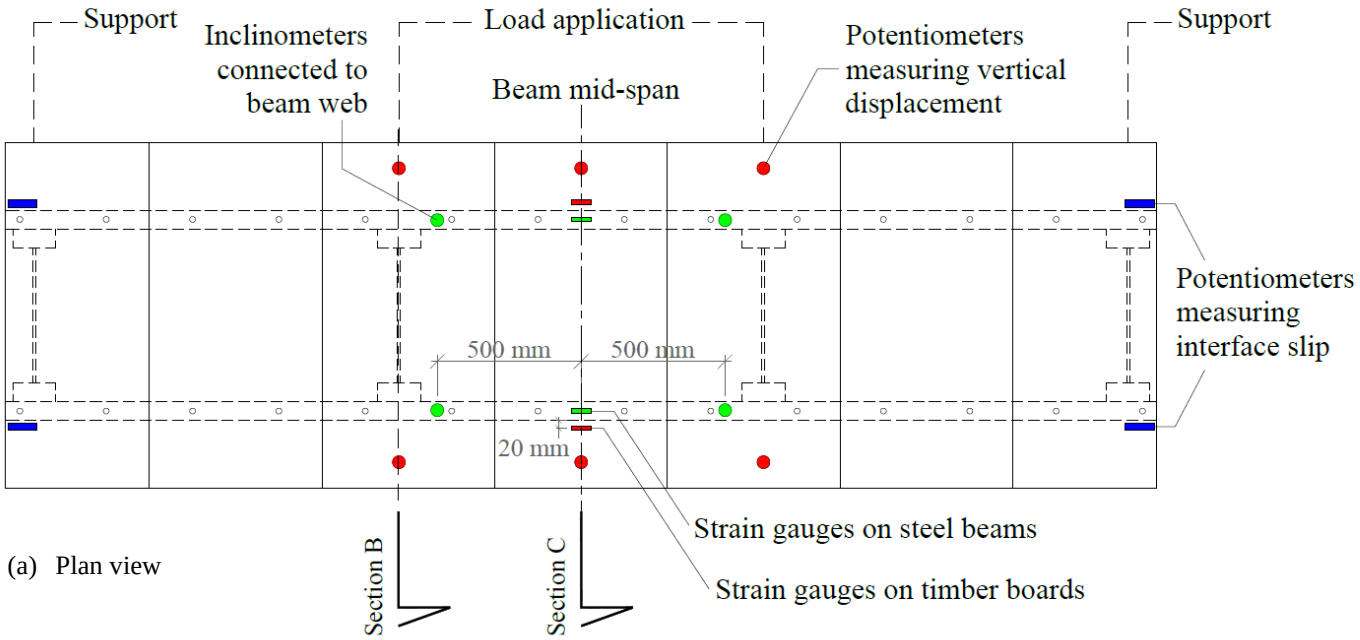

(a) Plan view

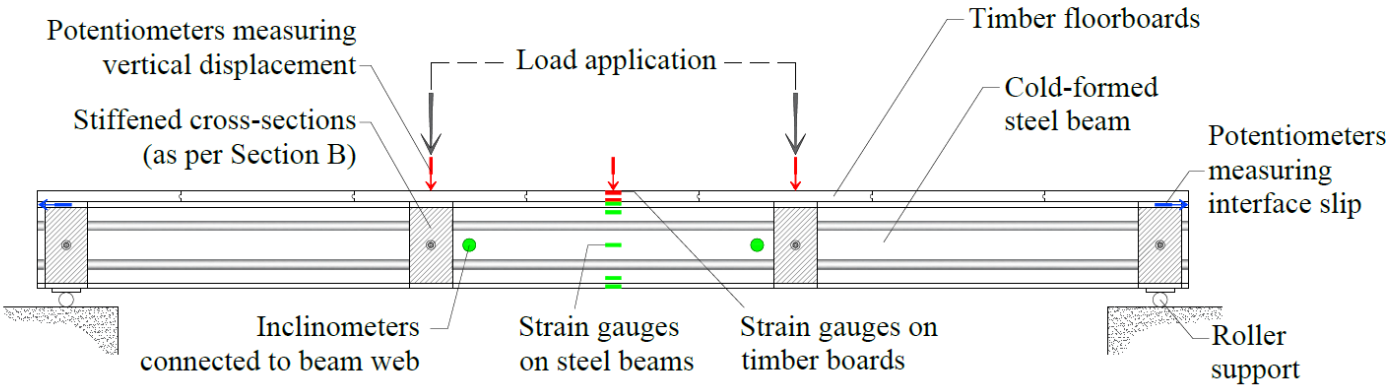

(b) Elevation

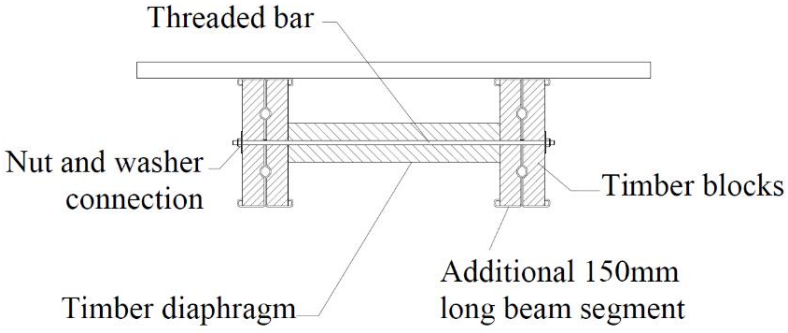

(c) Section B

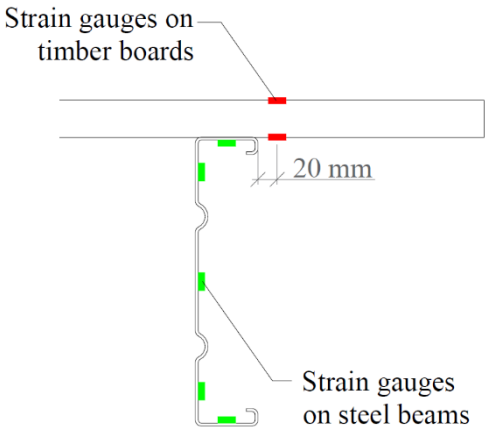

(d) Part section C

Fig. 9. Experimental layout – (a) Plan, (b) Elevation, (c) Section B, (d) Part section C

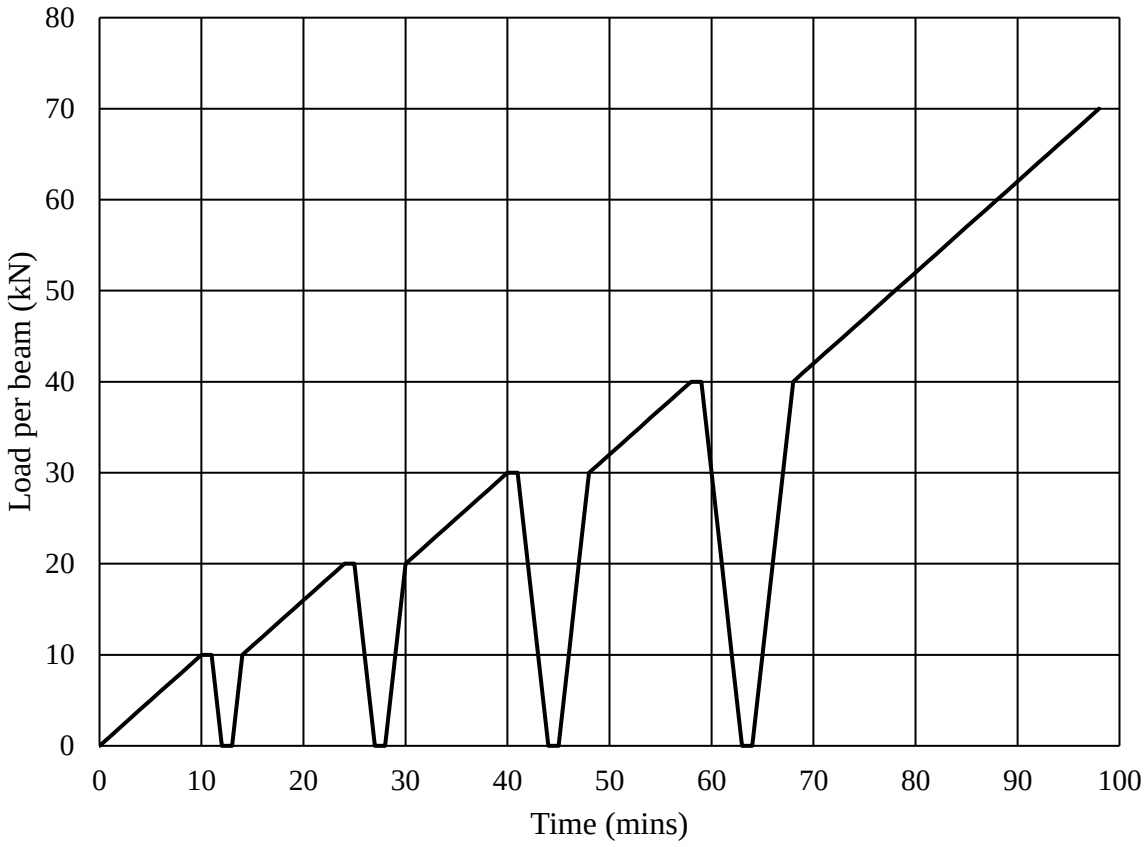

Fig. 10. Composite beam test loading procedure

Fig. 11. Minimising gaps by clamping new board to the one previously installed

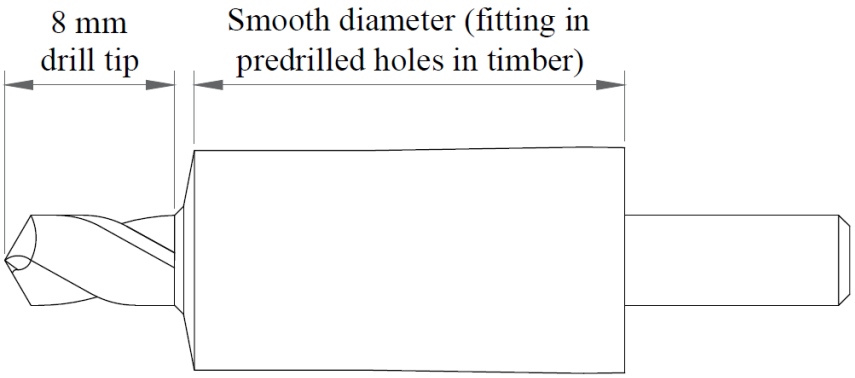

Fig. 12. Proposed drilling device to align the holes in the steel beam with those predrilled in the boards

Fig. 13. Failure of specimen No. 1 – Distortional buckling within the constant moment region

Fig. 14. Failure of specimen No. 3 – Distortional buckling within the constant moment region

Fig. 15. Failure of specimen No. 5 – Local buckling, with some distortional contribution, within the constant moment region

Fig. 16. Failure of specimen No. 5 – Local buckling, with some distortional contribution, adjacent to the connector

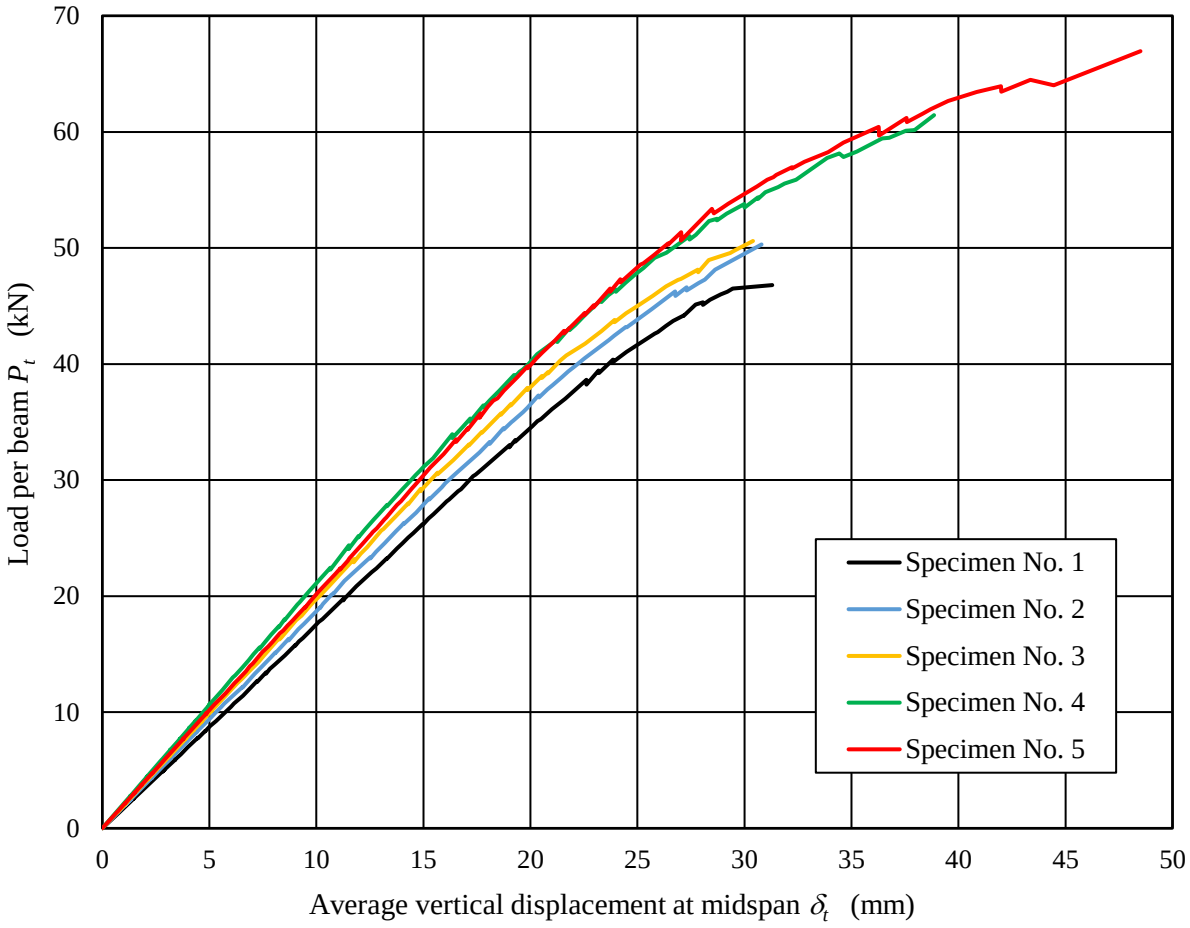

Fig. 17. Average load-displacement curves for composite beam tests up to ultimate load

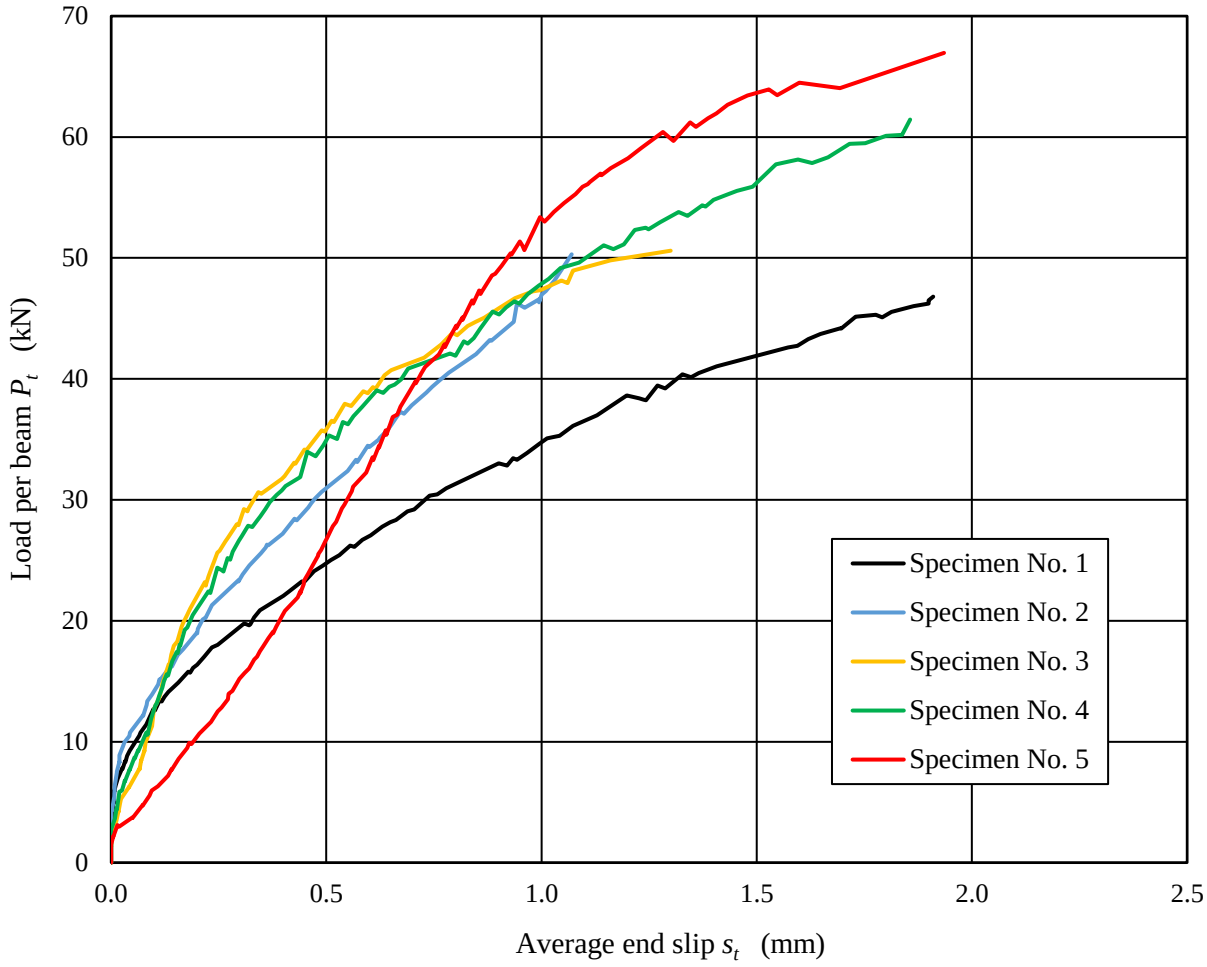

Fig. 18. Average load-end slip curves for composite beam tests up to ultimate load

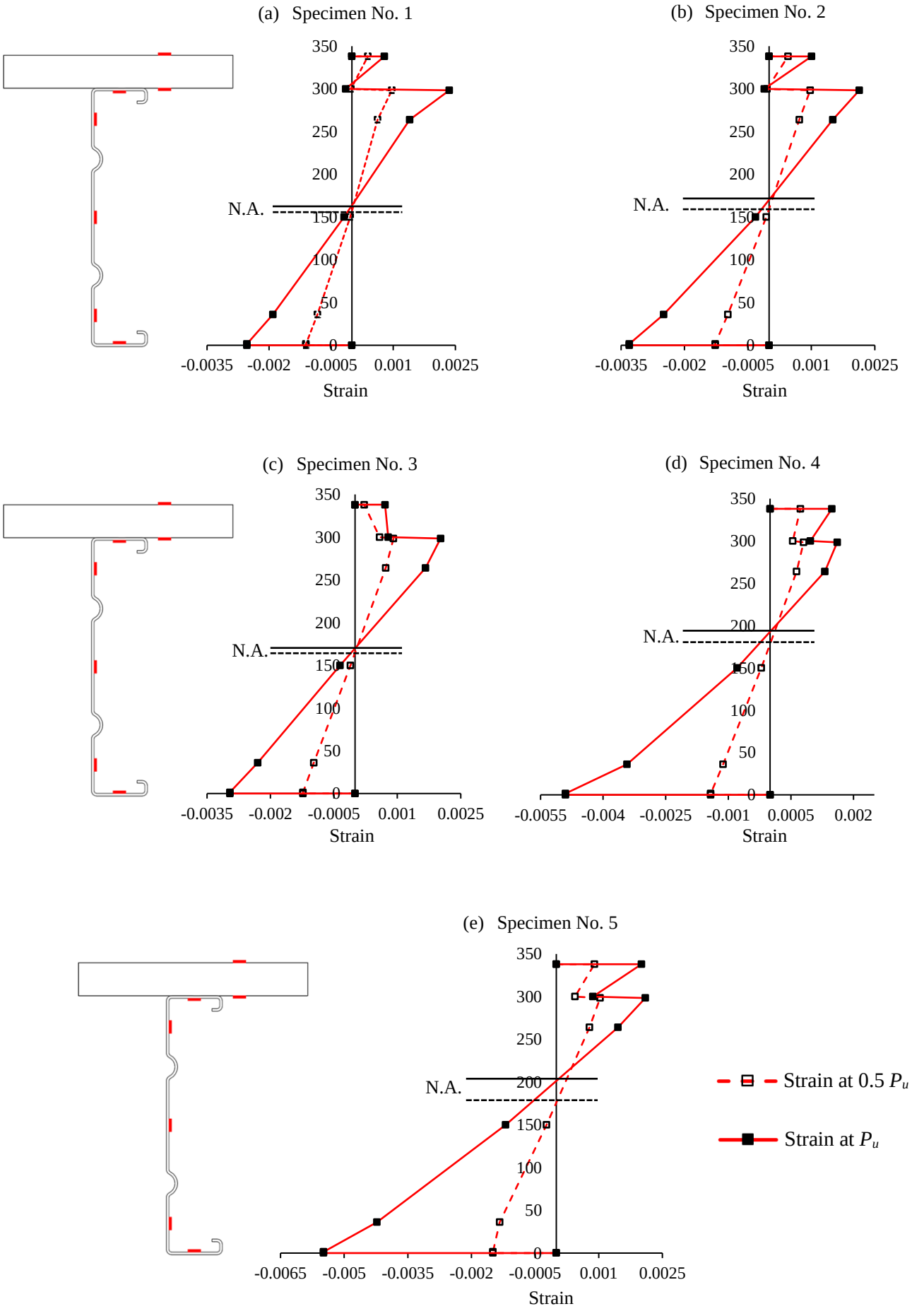

Fig. 19. Strain distributions at midspan

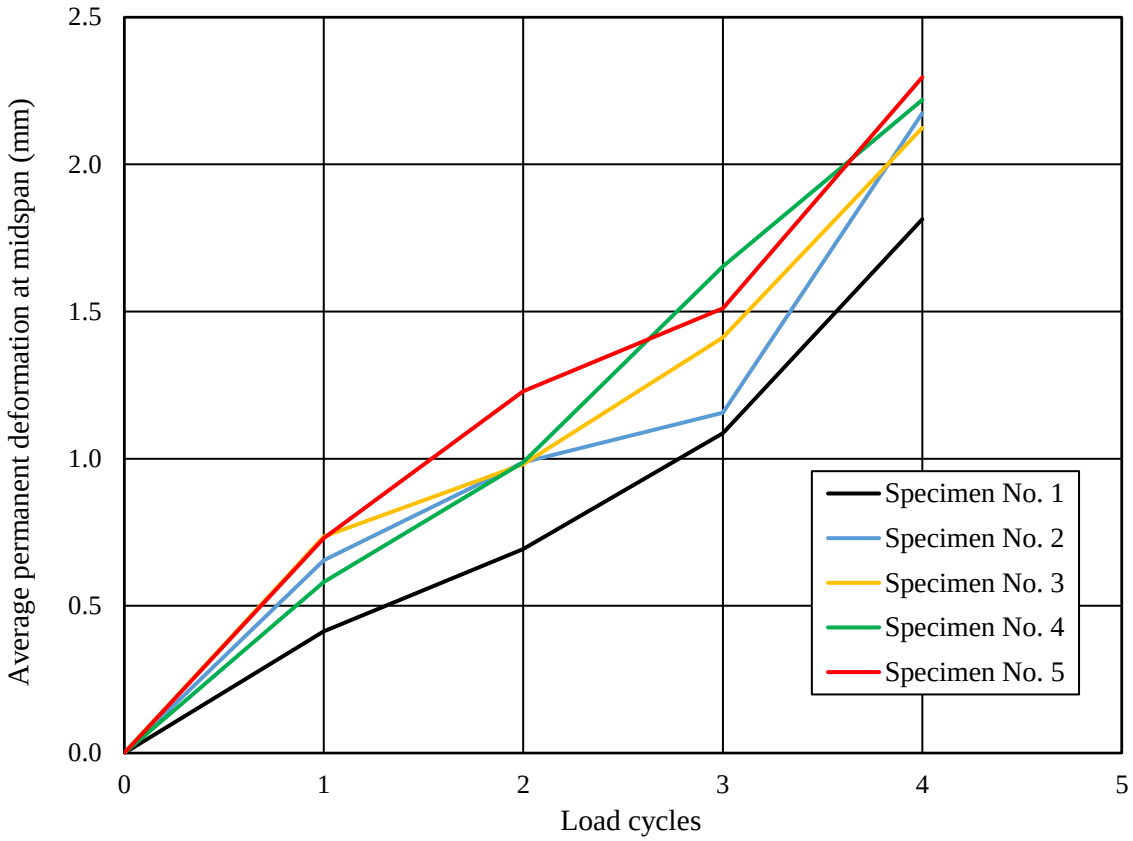

Fig. 20. Average permanent deformation at midspan after each load cycle

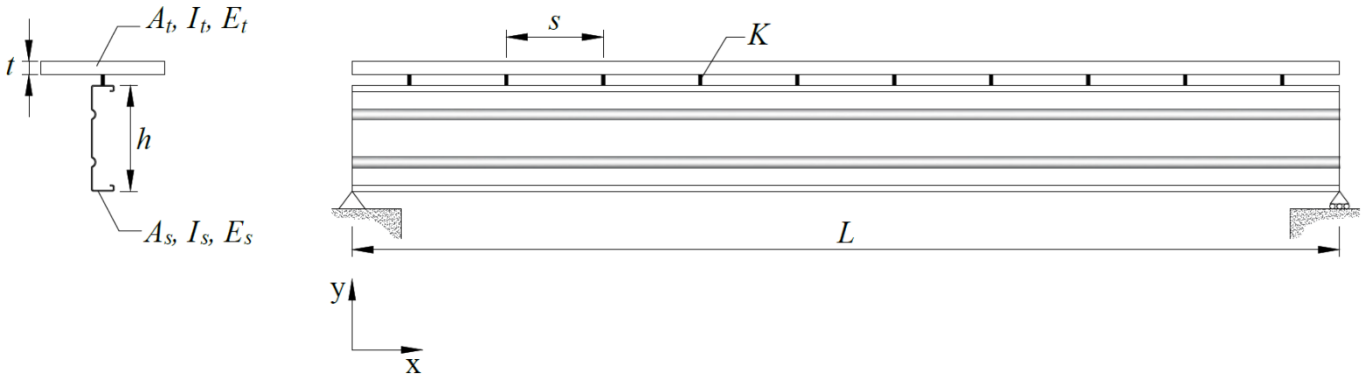

Fig. 21. Simply supported composite beam

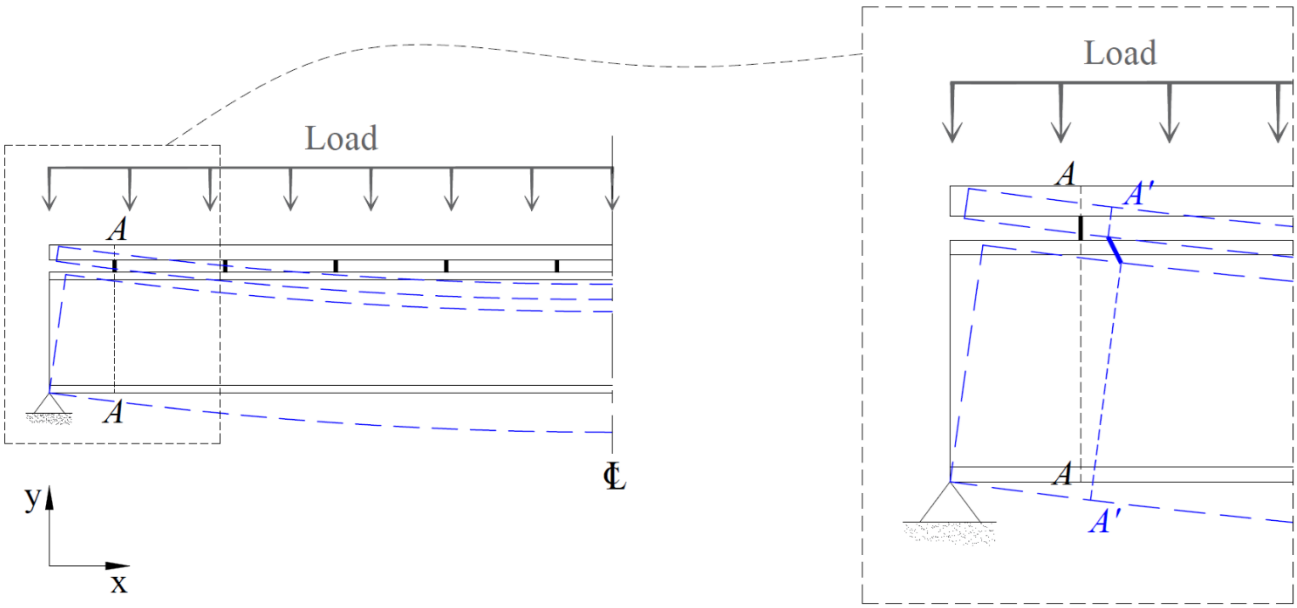

Fig. 22. Deformation of composite beam when subjected to vertical load

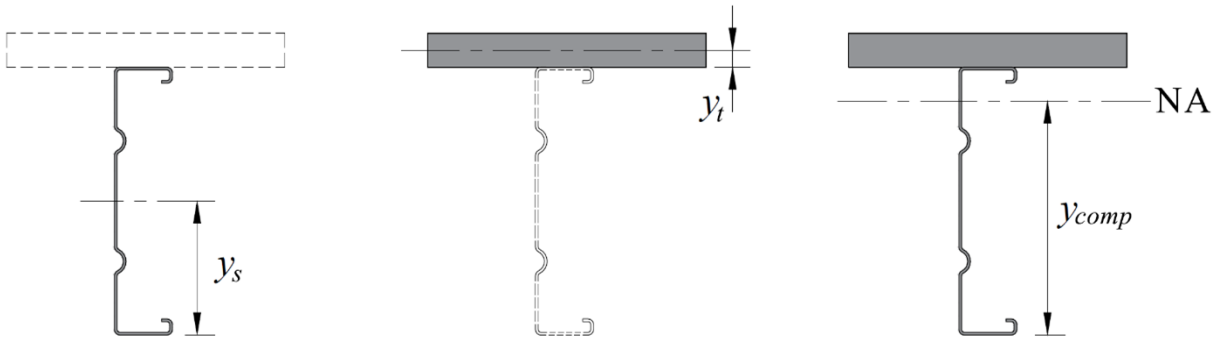

(a) (b) (c)

Fig. 23. Distance from centroid to base of (a) steel section, (b) timber board and (c) composite section with full shear interaction

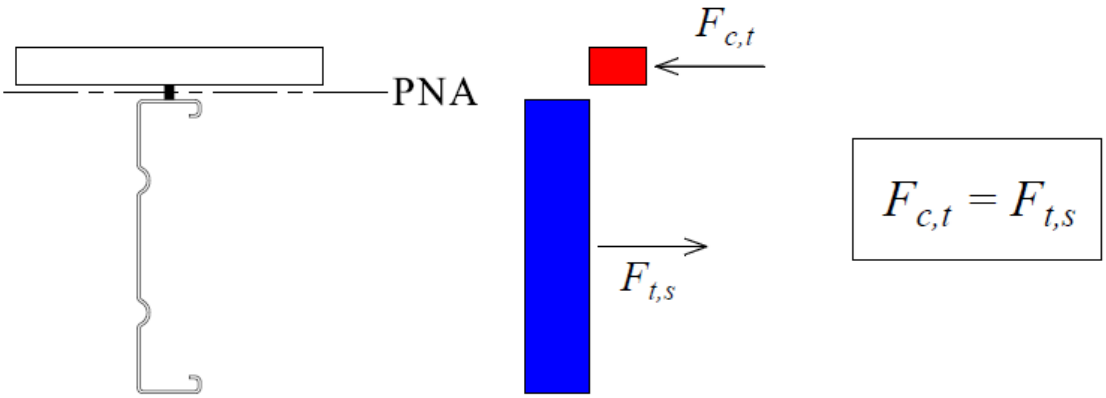

(a) Neutral axis at the beam-board interface

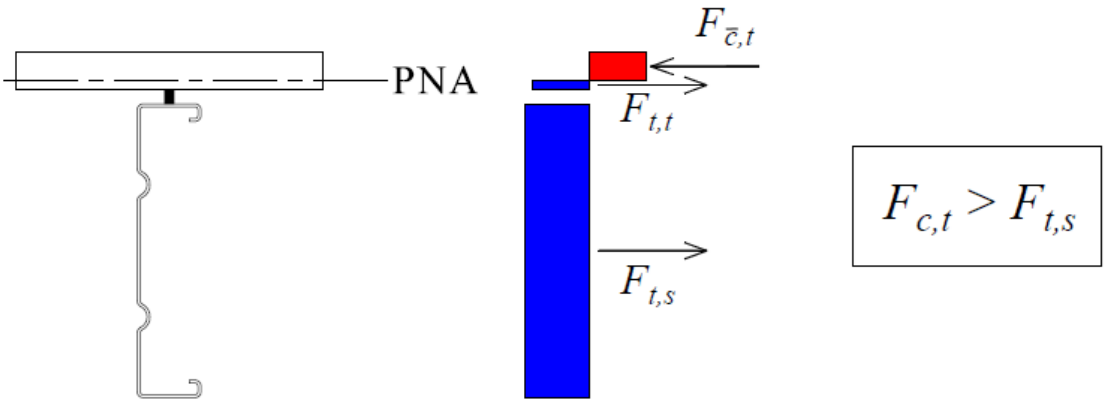

(b) Neutral axis within the timber board

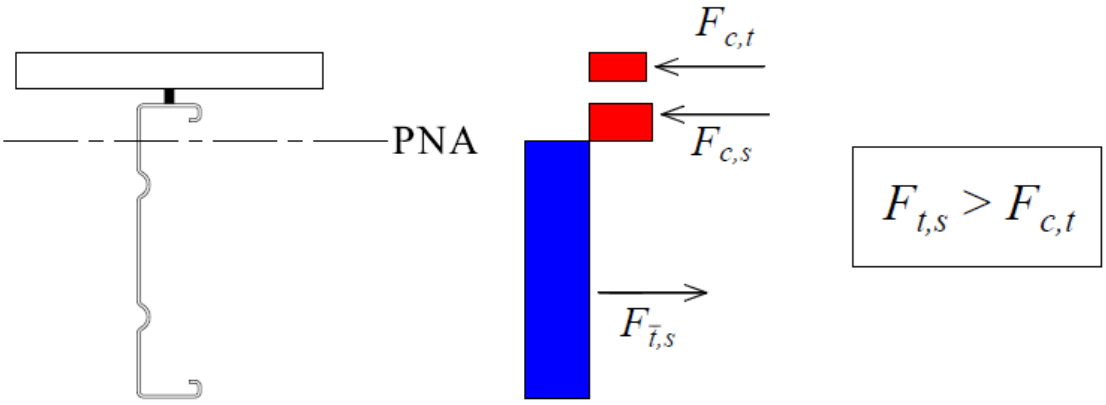

(c) Neutral axis within the CFS beam

Fig. 24. Longitudinal forces in a composite system with full shear connection.

Note that $F_{\bar{c},t}$ and $F_{t,t}$ are the compressive and tensile forces in the timber board respectively when the PNA lies within board. Similarly, $F_{c,s}$ and $F_{\bar{t},s}$ are the compressive and tensile forces in the CFS beam respectively when the PNA lies within beam.

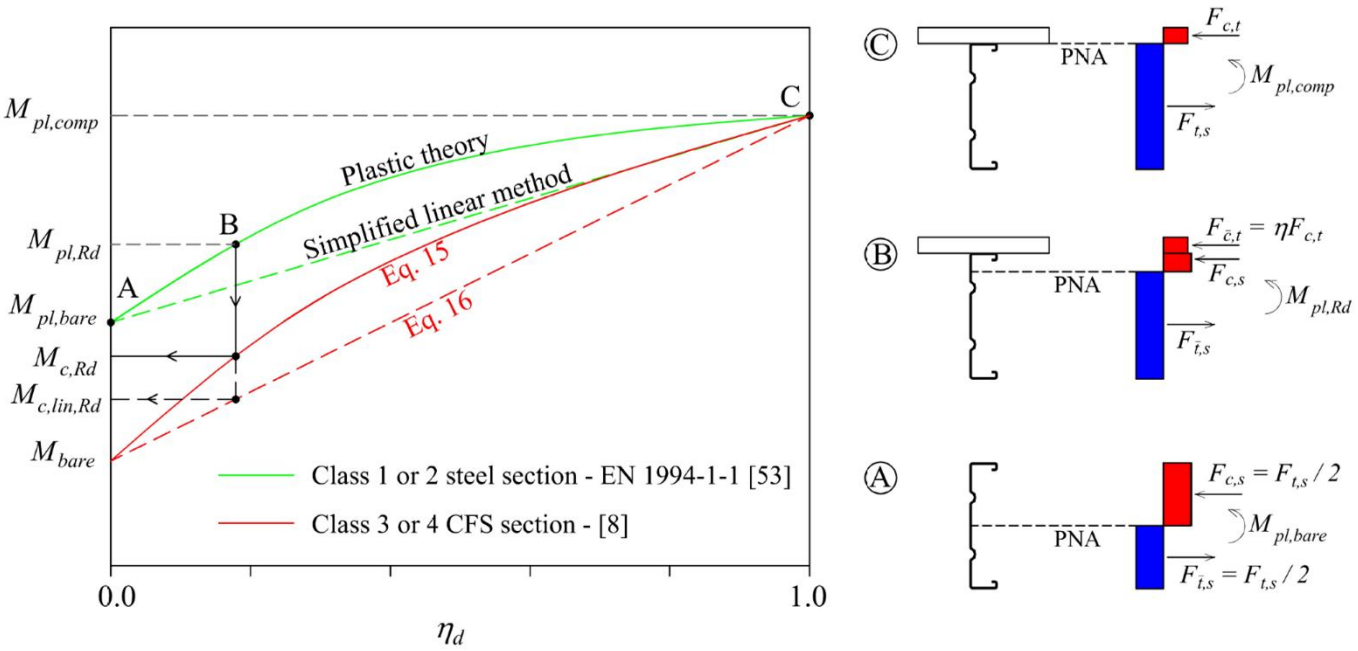

Fig. 25. Variation of moment capacity with degree of shear connection for a composite system with a Class 1 or 2 steel section – EN 1994-1-1 [53] and a Class 3 or 4 CFS section [8]